PSFC/RR-98-4 DOE/ET-51013-329

Alternate Methods of Vertical Plasma Control in the Alcator C-Mod Tokamak

G.H. Miller

Plasma Science and Fusion Center
Massachusetts Institute of Technology
Cambridge, MA 02139

May 1998

This work was supported by the U. S. Department of Energy Contract No. DE-AC02-78ET51013. Reproduction, translation, publication, use and disposal, in whole or in part by or for the United States government is permitted.

ALTERNATE METHODS OF VERTICAL PLASMA CONTROL IN THE ALCATOR C-MOD TOKAMAK

by

ENS GEORGE HUGH MILLER, USN

B.S., Systems Engineering
United States Naval Academy (1996)

Submitted to the Department of Nuclear Engineering
in Partial Fulfillment of the Requirements for the Degree of
Master of Science in Nuclear Engineering

at the

Massachusetts Institute of Technology

June 1998

Signature of Author .....
Department of Nuclear Engineering
May 8, 1998

Certified by .....
Ian H. Hutchinson
Thesis Supervisor

Accepted by .....
Lawrence M. Lidsky
Chairman, Department Committee on Graduate Students

ALTERNATE METHODS OF VERTICAL PLASMA CONTROL IN THE ALCATOR C-MOD TOKAMAK

by

ENS George Hugh Miller

Submitted to the Department of Nuclear Engineering
on May 8, 1998 in Partial Fulfillment of the
Requirements for the Degree of Master of Science in
Nuclear Engineering

ABSTRACT

This thesis investigates alternate methods of controlling the vertical position of the plasma in the ALCATOR C-Mod Tokamak. The purpose of this work is to examine alternative methods of controlling the plasma position that can be adopted to improve performance over the current system, which uses a proportional-derivative (PD) control system actuated through a pair of outboard equilibrium field coils (EFC). The first part of this investigation examines the possibility of using inboard ohmic heating coils (OH2) as the controlling coils. A coupling transformer was designed to connect a large amperage/low bandwidth power supply to a small amperage/high bandwidth power supply, removing the need for an expensive large and fast power supply. Both PD control laws and full state feedback laws were also compared for performance. A rigid displacement model of the plasma motion was developed that took into account a model of induced currents in the vacuum vessel and coils.

The results of the analysis concluded that there were moderate speed advantages to using state feedback on The OH2 coils, but these were outweighed by the robust operation of EFC PD control. No design achieved a decisive margin of improvement over the current control system.

Thesis Supervisor: Ian H. Hutchinson
Title: Professor of Nuclear Engineering

Contents

ACKNOWLEDGMENTS

I would like to thank several people for their help and support. The first is professor Ian Hutchinson, for giving me the benefit of instruction without which my work would not have been possible. I admire his professional example and keen perception. Several other people at the Plasma Science and Fusion Center have also provided assistance both large and small. Vincent Bertolino, Steve Wolfe, and Bob Granetz all took time out of their work to answer my questions. Donald Nelson responded wonderfully to my requests for computer support, and is single handedly responsible for making my programming efforts possible. Finally, Valerie Censabella always provided administrative help with a smile.

Many people both in Texas and Massachusetts gave me the family and community support that is necessary to complete two years of instruction at MIT. My parents provided a constant reminder that somebody loved me even when things looked tough. I would not know how to act without their respect and approval. My sister provided sibling support through her previous experiences and mind broadening conversations. My very large extended family was never short on praise and care packages. I do not believe many people have the opportunity to experience the support of over thirty people who want you to succeed. I would like to remember my cousin Henry Hall, who passed away during my last year in Boston. He was my only family in this state, and provided me with the sanity to survive the northern climate.

Major thanks goes out to my fellow graduate students. There are too many to list by name, but several people assisted me during my darker academic moments. The graduate crowd also provided me with the social life I needed to enjoy my time in Boston.

Final thanks goes out to the leadership of the United States Navy, who understands the benefits of higher education in the armed forces of America. Without official permission, my time here in Boston would have never occurred.

CHAPTER 1

INTRODUCTION

The most popular device used today in the quest for nuclear fusion is the tokamak reactor. So far, tokamaks have produced the best combination of confinement and temperature. Such results have allowed tokamak reactors to become the main thrust of magnetic confinement fusion research. The basic tokamak is a close field device that can be thought of as a circular solenoid bent into a torus. A vacuum vessel keeps atmospheric gasses from mixing with the hot plasma. Surrounding the vacuum vessel are magnetic coils used to control and augment specific areas of performance, including plasma confinement and positional stability. Figure 1.1 is a graphic showing the important parts of a basic tokamak design.

As new experiments have been developed, new ideas in the tokamak design have improved performance. Among those, the use of a plasma with an elongated cross section has been widely adapted. Elongated plasmas take the circular cross section of the basic tokamak and stretch it up and down to produce an oval shape. This improves two performance measurements used in tokamak engineering. β, defined as the ratio of plasma kinetic pressure to the confining magnetic pressure, expressed as

$$\beta = \frac{2\mu_o p}{B^2} \qquad \textbf{1.1}$$

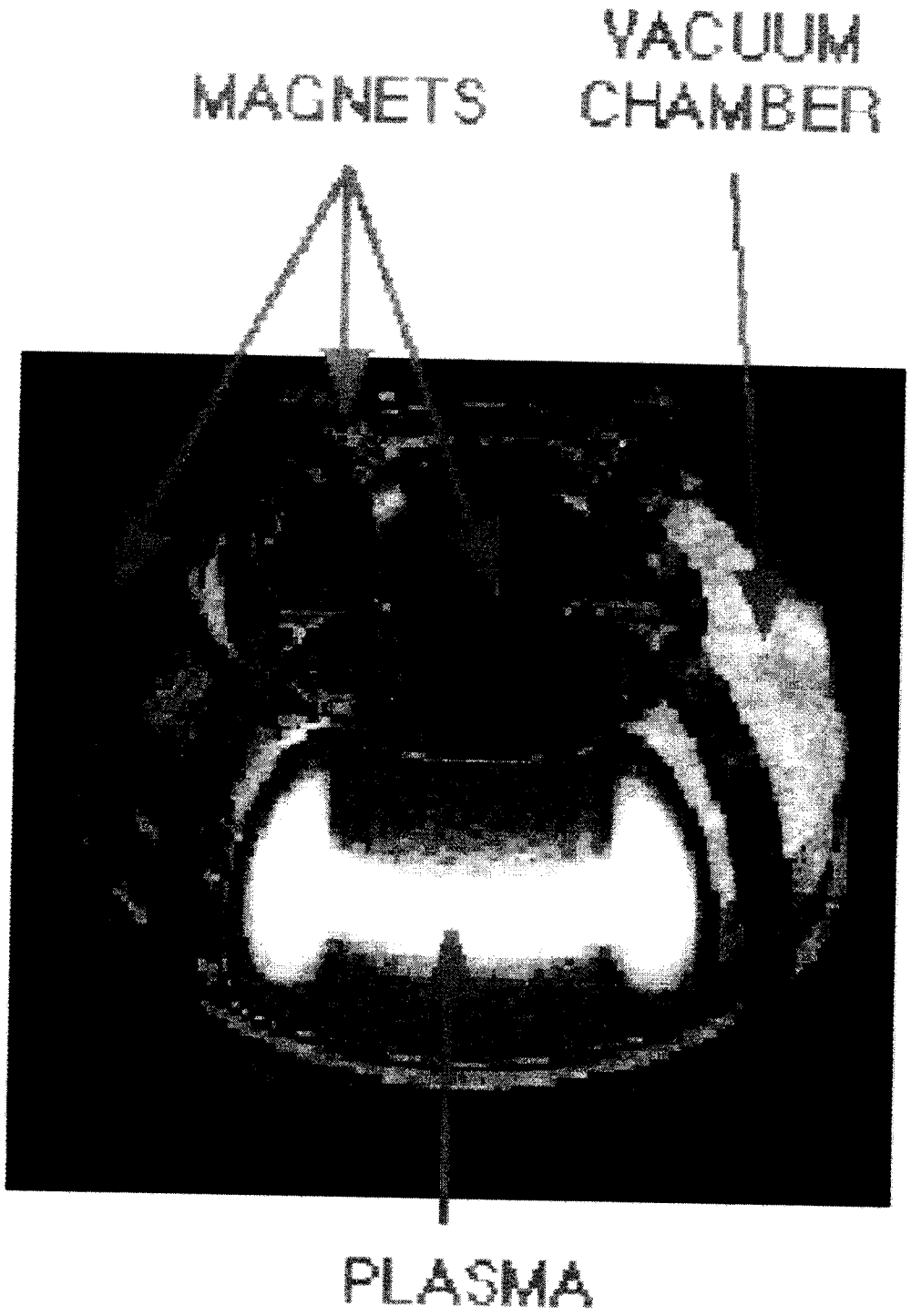

Figure 1.1 Basic Tokamak Parts
(From http://ippex.pppl.gov/**)**

is a measure of confinement efficiency that improves with elongated plasmas. They also allow a larger plasma current to improve particle confinement and plasma heating[1,2].

The next major tokamak design, which is hoped to produce a self-sustaining fusion reaction, has an elongated plasma cross section. One problem that this and other tokamaks have to plan for is the instability of the hot plasma in the vertical direction[3]. These vertical instabilities will move from their confined position in the center of the tokamak if left alone. To prevent this problem highly elongated plasmas require a special feedback control system[4]. The feedback control changes magnetic coil currents to push the plasma back in place if it observes the plasma moving away from a set position.

The amount of elongation in the plasma shape directly increases the β and plasma current benefits of the plasma. Unfortunately, highly elongated plasmas place extreme demands upon the power supplies used in a feedback control system[5]. Power supplies are an engineering limitation on the plasma elongation. An additional problem comes from the rapidly changing nature of plasmas. Standard feedback control systems are developed around a linear model set with specific plasma elongation and current. If these parameters change, the feedback control may not be able to continue stabilizing the plasma. A feedback control system that can continue to stabilize the plasma under the range of plasma conditions reached in operation is defined as a robust system. This thesis studies possible improvements to the ALCATOR C-Mod control system to overcome the engineering limitation on elongation while improving the robustness of the system.

Control of the vertical instability is realized by having two coils on opposite sides of the equatorial plane. The controlling power supply maintains antisymmetric currents in the

coils that are changed to affect the vertical position of the plasma. The ability of a coil pair to move the plasma is determined by placement geometry. For this investigation, coil positions examined are fixed according to the completed design of ALCATOR C-Mod tokamak. Experiments on the TCV tokamak have suggested that the best coil placement for fast control is inboard close to the equatorial plane [6]. This is in contrast to our device, which currently uses a pair of outboard coils (EFC) to stabilize the vertical instability.

To realize inboard control advantages on the ALCATOR C-Mod tokamak, vertical position control has to be done with the OH2 coils. Currently the main purpose of the OH2 coils is to drive current in the plasma. This provides for an ohmic source of plasma heating and gives the plasma an initial current. To achieve acceptable results, the OH2 coils require power supplies with high current. Unfortunately, the current power supplies do not have a quick response time to control fast vertical instabilities. Purchasing power supplies that have the necessary speed and amperage would be prohibitively expensive, and an alternative is required. It is proposed that a fast power supply be coupled with the current OH2 power supplies by a transformer. This allows the OH2 coil to have the necessary response speed for vertical position control without sacrificing the amperage needed for its other purposes.

Besides examining different coil positions, alternate control methods are considered for improving the control over the vertical position. The current ALCATOR C-Mod control system provides PID control for the plasma vertical position. It does not use modern control theory methods to improve robustness or reduce control signal magnitude. An alternative is the use of full state feedback (FSFB), which requires that all the information of the system represented in a

state variable model be used in feedback laws. It allows for more flexibility in developing control gains for several optimal performance schemes[7].

The main obstacle to realizing FSFB in any system is the need for complete knowledge of the system states. If one is lucky, all of the states are measurable and FSFB can be implemented easily. This is not so with our system, where many states are inaccessible to the control theorist. The alternative is to use an observer, which predicts the system states from available measurements. Requirements placed on the observer include accuracy and noise rejection. Also, for our case observer development is limited by the prediction system available on the ALCATOR C-Mod control computer. A linear transformation of available measurements is used instead of a state differential equation model observer. If the linear transformation observer can work, it will prevent the need for purchasing a new control computer to realize FSFB.

1.1 RIGID DISPLACEMENT MODEL

To compare the proposed control options, an accurate model must be developed. An acceptable approach for the vertical stabilization of an elongated plasma in an air core tokamak is the rigid displacement model[8]. This model takes into account the mutual inductance and resistances of the vacuum vessel and coils. The vacuum vessel and coils are represented as a continuous longitudal loop filament that can be subdivided to increase accuracy. This is limited by the practicality of developing FSFB for a system with too many states. Chapter 3 covers solutions to this problem in creating a working model.

The rigid displacement model does not provide for an exact representation of the plasma. Like the vacuum vessel and coils, the plasma is represented as a continuous longitudal filament. Current in the plasma is assumed to be constant for the calculation. Movement is limited to rigid displacements in the vertical axis. The plasma mass is ignored to remove the plasma velocity state. These conditions lead to a model that represents the plasma as being instantaneously in MHD equilibrium. The plasma is coupled to the remaining conductors by a circuit equation. Several ways for combining the equilibrium condition with the circuit equations were used to test specific control theories. Derivation of these models is included further in this thesis.

1.2 POWER SUPPLY MODELING

The effects of power supplies on the control system are not extensively modeled. For the initial investigation power supply dynamics were not included in the control calculations. Since the chopper power supply is the only system available for vertical control, it is assumed that power supply dynamics would not matter for comparisons of the control options. This allowed for easy development of several initial control systems. As a consequence of ignoring the power supply dynamic the control systems have infinite bandwidth. Since this is not possible with real components, the developed control systems produce unrealistic results. To impose an arbitrary frequency cutoff, a single pole power supply model is inserted into the control loop. This is not an accurate representation of the highly nonlinear Chopper power supply, but it does prevent the control systems from achieving artificial perfection.

The other power supplies are not used for vertical control, so their effects were modeled with a much simpler method. During plasma operation the remaining power supplies work to maintain preset currents in the coils. This process was modeled as an increase in the coil resistances, which reduced the ability of the control system to change coil currents in the model through induction. Finally, having a complete model of the transformer coupled power supply is important in the realization of OH2 vertical mode control. Such a model is beyond the scope of this work. However, the level of modeling present allows for a decision to be made on the viability of an OH2 vertical control system.

1.3 COMPARISONS BETWEEN CONTROL SYSTEMS

Since the design of this thesis is to examine several control systems, methods of comparison must be researched and developed. General criterions for the systems include mathematical soundness and ability to stabilize vertical displacements. Beyond these requirements is specific quantification of control system performance. In the linearized model, this includes the size of the control gains needed to produce an acceptable settling time for vertical displacement corrections. Since the linear model works only for a specific set of input conditions, the effect of a change in plasma conditions must also be examined. The designed control systems were examined for their ability to stabilize vertical displacement over a range of plasma elongations. The qualification for adoption of a new control method is an order of magnitude improvement over the current system.

1.4 SUMMARY

This thesis will investigate new methods of axisymmetric control on the ALCATOR C-Mod tokamak. The advantages and disadvantages of these methods will be compared with the current system to decide a possible replacement.

Chapter 2 covers the proof of the transformer coupling idea. Stress, thermal, and electrical requirements are examined to decide the feasibility of construction. Additional requirements for realizing a design are mentioned, but full analysis is left for additional research. Chapter 3 describes the forms of the rigid displacement model used. It includes a full derivation of the model and a look at variables important to the analysis of the control system. Chapter 4 includes an introduction to the control methods used in this thesis. Both PID and FSFB methods are included. In chapter 5 the results of comparisons between the different types of control systems are presented and described. Chapter 6 ends with conclusions and suggestions for additional research that did not fit into the current investigation.

CHAPTER 2

THE TRANSFORMER

The transformer as conceived allows for the insertion of a smaller and faster power supply into the OH2 coil power supply circuit. The large power supply provides the size of current needed for ohmic heating while the smaller power supply will have the response time necessary to control the vertical mode. A more straightforward solution would be to purchase a new power supply for the OH2 coils that have a high current and large bandwidth. This option comes with to high a price though, and using as much equipment already on hand is preferable. Economics and efficiency are the reasons a coupled two power supply systems is being investigated.

The plan investigated is as follows. The transformer will hook up one chopper power supply to both the upper and lower OH2 coils. One primary will be connected to two secondaries in the OH2 power circuit. The control signal is applied to both coils in anti-series, which the suggested arrangement allows with the use of just one fast power supply. This fast power supply will provide for quick changes in the difference of the OH2 coil currents to stabilize the vertical mode. The slower power supply will have feedback response with the purpose of centering the error signal of the fast power supply. By this method, saturation of the actuating signal on the fast power supply can be avoided.

Strains placed on the transformer are high. The secondary loops have a large DC current (>30,000A) that must be accounted in the design. This effectively introduces a DC bias that saturates all core materials. An air core design is seen as the best option, as the advantages of an iron core are negated by the secondary current. Also, an air core design gives advantages by not having to consider iron core losses and the need to cool the extra mass of metal. In addition, the large current lends our device to pulse operations, as the cooling requirements to achieve steady state operation would be a serious engineering problem. Since ALCATOR C-Mod is a pulsed experiment, the transformer can be designed not to place any constraints on machine operation.

As far as the author knows, the attempt to use a coupling transformer in its designed configuration is unique. Full design of the transformer and its effect on the control system is a complex question that will not be covered in this work. This chapter is a proof of the concept, with specific details omitted. Four areas are covered:

1. Circuit Requirements, including voltage, and current limits.
2. Thermal Requirements, describing the method of inertial cooling.
3. Structural Requirements, an analysis of the forces developed on the transformer.
4. Magnetic Requirements, looking at the flux needed to provide adequate coil control

The concerns of eddy losses and dielectric breakdown are cursorily examined as subjects that are important to building the transformer.

2.1 CIRCUIT REQUIREMENTS

The main concern is the effect of the second power supply on the Poloidal coil system of the ALCATOR C-Mod tokamak. If attaching a fast power supply to the OH2 coils damages any of the coils, then the transformer idea would be useless. Our main concern is the potential for direct or induced voltages to damage a coil or trip a fault system. On the other hand, high voltages allow for the control system to change the current quickly despite high inductances. Varying the turns ratio of the transformer allows the voltage transferred to be adjusted within preset ranges.

A lower limit to voltage transferred is established by placing a limit on the maximum number of volts that can be sent into the coils. Using Kirchoff's voltage law on the circuit in figure 2.1 gives us an inequality that sets the maximum voltage applied to the coils,

$$V_{OH2} + V_{SEC} \leq V_{LIM} \qquad \textbf{2.1}$$

V_{oh2} in equation 2.1 refers to the voltage produced from the OH2 power supply, V_{sec} is the voltage coming from the secondary coils, and V_{lim} is the maximum allowable voltage across the OH2 coils. The voltage from the OH2 power supplies and the secondary of the transformer cannot exceed the coil limits. We define our turns ratio, N, as the primary turns over secondary turns and replace V_{sec} with V_{pri} to give us the relation where

$$N > \frac{V_{PRI}}{V_{LIM} - V_{OH2}} \qquad \textbf{2.2}$$

This sets a lower bound on the turns ratio. There is no pressing need to establish an upper bound on the turns ratio. Since the main concern is with having a fast power supply, keeping the turns ratio less than one is beneficial. On the other hand, a turns ratio greater than one would allow our power supply to produce a current gain that would apply more force to the plasma. The turns ratio cannot be optimized until a careful analysis of the needed control response is determined.

The next constraint of the design is the voltage effect it will have on the other coils in the ALCATOR-C Mod tokamak. Mutual inductances between each coil are used to determine the voltages induced by the fast power supply. The mutual inductance matrix, $\boldsymbol{M}$, describes the flux linkage between all conducting elements. An accurate derivation of $\boldsymbol{M}$ is also important in developing the rigid displacement model. To determine maximum induced voltages the OH2 coils are set in anti-series while the other Poloidal coils are assumed to be open circuits. Individual voltages are determined by the equation

$$V_i = \frac{\boldsymbol{M}_{ji}}{\boldsymbol{M}_{jj}} V_j \qquad \textbf{2.3}$$

where M is the matrix of mutual inductances, V_j is applied voltage, V_i is induced voltage, and I and j refer to the coil's position in the M matrix. When analysis was done, it was discovered that the largest induced voltage was on the EF1 coils. The factor is

$$V_{\mathrm{EFC}} \approx 1.6 V_{\mathrm{sec}} \qquad \textbf{2.4}$$

which will place an additional constraint on the maximum voltage allowed to develop across the secondaries.

2.2 THERMAL REQUIREMENTS

Normal transformer design concentrates on the steady state temperature during regular operation. This entails deriving the heat transfer properties of the transformer and solving for a maximum temperature at a particular hot spot. The calculations for the thermal properties on this transformer are made much easier because of the short time of operation. The rapid heat generation in the copper dominates over the heat transfer term, leaving conventional transformer heat calculations unnecessary. Instead, we consider the use of inertial cooling for the copper wire of the primary and secondaries. Technically, the coil is not cooled at all. The wire is made thick enough so the copper present can hold all of the heat generated during a pulse without failing. Heat is considered to be generated exclusively from the I^2R losses, as this is the dominant term. Other losses in the transformer can also add heat, but they are ignored for now. Mention of them is made in section **2.5**.

Determining the cross section dimensions of the turns comes from the heat capacity of the copper conductor. A general formula to calculate the temperature rise in a pulsed conductor without heat transfer is

$$\int_{T_1}^{T_2} \frac{C_v}{\eta} dT = \int_{t_1}^{t_2} j^2 dt \qquad \textbf{2.5}$$

where C_v is the volume heat capacity, η is resistivity, j is current density, T is the temperature, and t is the time[9]. If the following linear relationship for the temperature dependence of η is used,

$$\eta = \eta_{300} \frac{(T-50)}{250} \qquad \textbf{2.6}$$

then it allows for the left side of the equation to be integrated. Setting t_1 to 0, a formula for the acceptable $(A/m^2)^2$s is developed,

$$\int_0^t j^2 dt = \frac{C_v 250}{\eta_{300}} \ln\left(\frac{T_2 - 50}{T_1 - 50}\right) \qquad \textbf{2.7}$$

that determines the maximum current density allowed for a given operating time and temperature change.

We have two options for this stage of the design, starting the coils at either room temperature or liquid nitrogen(LN_2) temperature. The room temperature coils begin with T_1=300K and the liquid nitrogen coils have T_1=80K. The final allowed temperature is set at a reasonable 325K for the room temperature coils. On the LN_2 cooled coils we set the final temperature lower at T_2=300K,. The design parameters assume a pulse time t=2 sec, a constant current of 30,000 Amps in the secondary, and a constant current of 1500 Amps in the primary. For a room temperature design the transformer needs a 2.6x 2.6cm^2 square secondary and a .6x .6cm^2 square primary cable at a minimum. The LN_2 temperature coils need 1.2x 1.2cm^2 for the secondary cross section and .3x .3cm^2 in the primary. Since these are the minimum areas required to stay within the designated temperature range, a safety factor of 3 in cross section is suggested to cover situations above the design conditions. This expands the dimensions to 4.5x 4.5cm^2 secondary with 1.0x 1.0cm^2 primary for room temperature and 2.0x 2.0cm^2 secondary

with .5x .5cm^2 for LN_2 temperatures. The substantial size of the secondary if the transformer starts out at room temperature suggest that a liquid nitrogen cooled transformer is the best option.

2.3 STRUCTURAL REQUIREMENTS

There are two types of forces that concern this design, the outward pressure on the transformer and the interwinding forces between the wires. These forces are a consequence of having a current in a magnetic field. The transformer can be modeled as two solenoids placed together, giving us our magnetic field represented by

$$B=\mu_0 nI \qquad \textbf{2.8}$$

The n in this equation refers to the number of turns per meter[10].

Hoop stress σ_H in a solenoid due to the IxB force is defined as

$$\sigma_H=\frac{BIna}{2w} \qquad \textbf{2.9}$$

where w is the thickness and a is the radius of the solenoid[11]. Combining equations 2.8 and 2.9 to remove the I term gives us

$$\sigma_H=\frac{B^2 a}{\mu_0 w} \qquad \textbf{2.10}$$

which is the stress on a solenoid caused by the B field. With the thickness, w, initially determined by the size of the conductor needed, equation 2.10 describes the maximum hoop stress for a given radius of transformer design.

The interwinding force per unit length of the circumference can be roughly estimated as the force between two current carrying wires,

$$F=\frac{\mu_0 I_1 I_2}{2\pi d} \qquad \textbf{2.11}$$

with d representing the distance between the centroid of the two wires and F equal to the force per unit length[10]. For our worst case scenario the current in the two secondaries may peak at 50,000 Amps. An initial calculation with $I_1=I_2=50{,}000$A and d≈3cm apart, gives a force per unit length of 16,700 N/m. Distributed over the width of the secondary gives us a compressive pressure of .8MPa between two turns. A more thorough derivation is necessary to find the exact forces between each turn of the primary and the secondary, but the initial calculation shows that interwinding forces are within a range that can be accommodated by reasonable mechanical design.

The structural requirements listed here are used to decide if a transformer design will exceed standard yield strengths for available engineering materials. Cyclic fatigue and thermal expansion are not considered in this paper. A full analysis would contain a design for a restraining structure that would account for both conditions.

2.4 MAGNETIC REQUIREMENTS

The total amount of turns needed and the required radius will be determined by the flux needed to be transferred through the transformer. Flux created by this transformer is determined through geometry and number of turns per meter. The flux in the OH2 coils that needs to be changed can be roughly considered as a product of the current in the secondary and inductance of the OH2 coils, shown as

$$\Lambda = M_{jj} I \qquad \textbf{2.12}$$

where Λ is the flux linkage. Using our values for the chopper peak swing current in the secondary I=750A, inductance $M_{22}=M_{33}=569\mu H$, and summing the flux for both OH2 coils give us a flux value $\Lambda=0.854 V \cdot s$. The volt second product produced by our solenoid is[12]

$$\Lambda = \mu_o \pi n^2 a^2 h I \qquad \textbf{2.13}$$

with h representing the height of the transformer. For a specified current and height, this equation provides a relationship relating radius to number of turns per meter. For later calculations the flux sent to other coils by mutual inductances will be added to find the total amount of volt seconds needed.

The next thing to be considered is the B-field produced by the DC voltage. While it will not transfer energy across the transformer, it must be considered for force calculations. Equation 2.8 gives us the B-field produced in a solenoid, and it is used to find the value of the magnetic field when the secondaries have their peak current of 50,000A. This will tell us the maximum B field that the mechanical part of the design needs to handle. An important thing to remember is that two secondaries are used in the calculation. A turns ratio of one has twice as many turns from the secondaries as there are from the primaries.

2.5 OTHER CONSIDERATIONS

So far our design has examined separate concerns that could have been preventing factors in realizing a coupling transformer design. Unfortunately, these considerations do not complete the full calculation requirements for our transformer. Two additional factors are mentioned that are important for completing the transformer. Also, the equations given do not fully optimize the design based on a cost and performance scheme. Several books with specific steps to achieve optimization exist, but the unique nature of this transformer does not lend itself to previously computed designs[13,14]. In addition, the J&P Transformer Book provides very detailed accounts of minor engineering considerations in the construction of a transformer[15].

Many additional losses complicate the final heat and electrical requirements. Eddy currents in the conductors are produced by the magnetic fields from the AC currents used in a transformer[14]. These show up as an additional AC resistance in a normal transformer. For this transformer, the power signal is far from sinusoidal, which adds additional higher frequency harmonics to the eddy current loss calculation. A paper by Phipps, et al. contains the necessary information for analyzing harmonics in the power signal[16]. Pierce provides a solid approach on how to consider these harmonics in transformer design[17].

Problems arising from the production of electric fields must also be taken into consideration. Dielectric breakdown in the insulation is an important engineering factor in final design. It is also possible that capacitive leakage due to potential high frequencies coming from the power supplies might exist. The most likely effect those considering electrical fields will do

to the design is increase the spacing between the coils when the required amount of electrical insulation is used. A good account of dielectric problems in transformers is given in [13].

2.6 POINT DESIGN

Armed with the information in this chapter, a preliminary design can be speculated. Liquid nitrogen cooled coils should be used to decrease the copper bar dimensions. Our secondaries will be a 2.0x2.0cm^2 bar and the primary will be a .5x.5cm^2 bar. Using the smaller size coils by cooling the copper is much easier to manufacture. The next important parameter is the turn ratio of the transformer. A turn ratio N=1 is specified for our first design. It has not been optimized for control performance, but it will provide a high voltage on the secondary that does not exceed the specified limits.

The next process is to determine the geometry. Equation 2.12 provides for an unlimited range of turns per meter and radius for the transformer. For this design we will use a spiral coil wrapping with the two secondaries and one primary taking up one layer. Keeping the conductors square and assuming 5 mm of insulation between the coils gives us a maximum number of turns per meter n=43. For this given amount of turns and a height h=1 meter the radius a=0.42 meters.

Using the other equations in this chapter a complete list of parameters are calculated and displayed in table 2.1. The resistive voltage drop across the secondaries is 10.5 Volts and across the primary is 13 Volts. All of the calculated parameters fall within a feasible range, showing the possibility of the transformer. Optimization of the design will be left as follow on work if the transformer is adopted.

Initial Transformer Design	
N Primary	40
N Secondary (2 coils)	80
V·s product	0.854
B Field (Tesla)	3.1
σ_H Stress (MPa)	56
Resistance Secondary (mΩ) @80K	0.35
Resistance Primary (mΩ) @80K	8.6
Height (m)	1.00
Radius (m)	0.42
Thickness (cm)	5.5

Table 2.1

CHAPTER 3

THE SIMULATION MODEL

To accomplish the goal of analyzing different vertical position control systems we need a method of simulating the process on a computer. This means representing the vertical instabilities as a set of equations that can be programmed into a computer simulation. Also, it is important that the representation allows for the development of feedback laws using existing methodology. Once these two requirements are met, the level of detail in the model has to be set. Simple models lack accuracy while more complex models become unmanageable. The rigid displacement model used was adapted to provide for these conditions.

The model uses a force balance equation to determine the vertical motion of the plasma. Since the currents in conducting elements make up a part of this force balance equation, a circuit equation is needed to relate current dynamics to the position of the plasma. These two sets of equations can be combined to create a system of first order differential equations. This system of equations can be easily programmed into a simulation or solved as a generalized eigenvalue problem.

3.1 BASIC TERMS

Before the model can be fully described, it is important to introduce a few terms to describe the tokamak machine and plasma. The geometry of the model is shown in figure 3.1. The position of conducting elements and the plasma in the machine are described by standard cylindrical coordinates (R,ϕ,Z). For normal tokamak equilibrium the position of the plasma is considered independent of the toroidal angle, ϕ. Also, the conducting elements are axisymmetric to the toroidal angle, allowing the model to be described in the (R,Z) plane.

The elongation of the plasma is defined as

$$\kappa \equiv l_y / l_x \qquad \textbf{3.1}$$

where l_y is the vertical axis and l_x is the horizontal axis of the plasma. The axis are shown in figure 3.1. An elongation factor greater than one indicates the degree that the plasma is stretched in the vertical direction. As mentioned in the first chapter, high elongation, represented by a large κ, corresponds to improved performance measurements in a tokamak.

The rigid displacement model looks at the interaction of the plasma current with other currents in the tokamak. This consists of currents induced in any conducting structures and those produced by the power supplies in the magnetic coils. Instead of representing the currents by a profile through conducting structures, they are modeled as single currents flowing in circular filaments in the (R,Z) plane. The advantage of a filament model is that the number of filaments can be increased to provide for higher accuracy or decreased to reduce computation time. 50 filaments were used in the conducting filament model to calculate the vertical displacement growth rates.

3.2 FORCES ON PLASMA

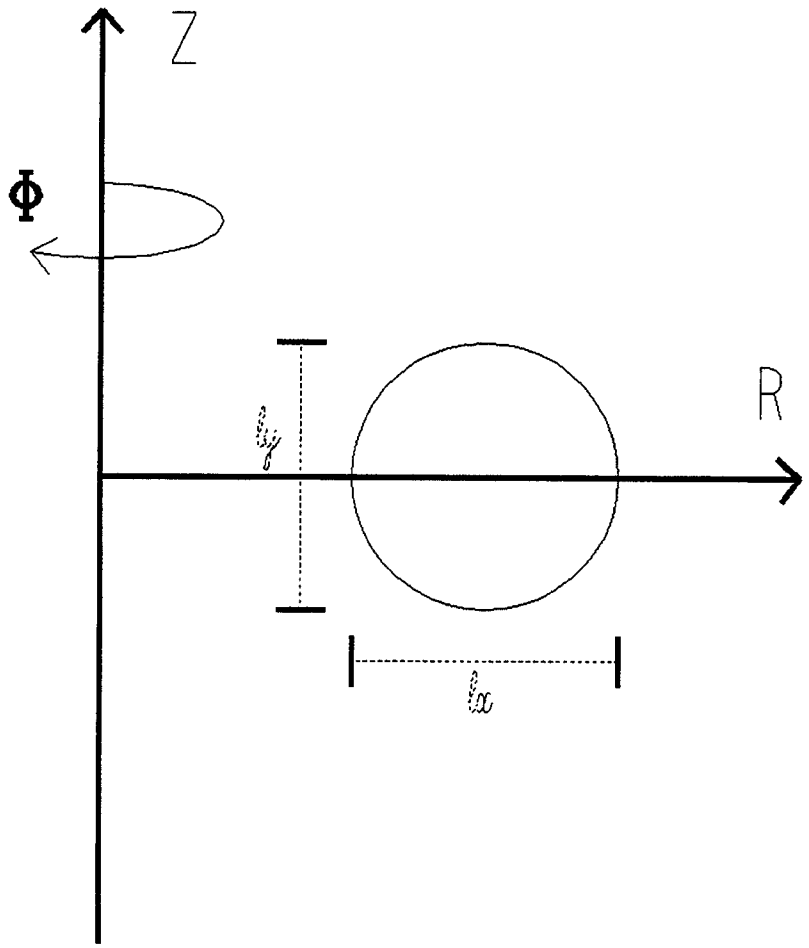

Figure 3.1 Coordinate System

The simplest way to model the plasma motion is to create an equation of the form

$$m\ddot{z} = \Sigma F_z \qquad \textbf{3.2}$$

where ΣF_z is the sum of forces in the z direction, m is the plasma mass, and $\ddot{z}$ is the acceleration of the plasma in the z direction. By determining the various forces acting on the plasma, a reasonable model of motion in the z direction can be derived. Unfortunately, not all of the F_z equations are functions of z or t (time), meaning that equation 3.2 cannot be solved without additional dynamics added. These will be described in the next section and combined with equation 3.2 to produce a system of first order equations.

There are two forces used in equation 3.2. The first force is caused by the magnetic fields that produce an elongated plasma. In order to create an elongated plasma, a quadrupole magnetic field is superimposed upon the poloidal field of the tokamak. The gradient of this magnetic field creates a force on the plasma filament given by

$$F_{DI} = -2\pi R_p I_p \frac{\partial B_r}{\partial z} z \qquad \textbf{3.3}$$

where F_{DI} is the force term caused by the field, R_p is the major radius of the plasma, I_p is the plasma current, B_r is the magnetic field in the radial direction, and z is the vertical displacement along the Z axis. With I_p defined as positive, the force will push the plasma away from the center if the gradient of B_r is negative. This is the case when the quadrupole field is added to produce a vertically elongated plasma. The gradient of B_r can be replaced by the decay index, n_i, which is used to describe the field curvature. The force in the z direction is then written as

$$F_{DI} = 2\pi I_p n_i B_{z0} z \equiv S_B z \qquad \textbf{3.4}$$

where n_i is defined as

$$n_i \equiv -\frac{R_p}{B_{z0}}\frac{\partial B_r}{\partial z} \qquad \textbf{3.5}$$

The vertical field, B_{z0}, is evaluated for the position of the plasma. B_{z0} is determined by a set of equilibrium conditions to prevent radial expansion. The larger the decay index, the more unstablizing F_{DI} becomes to the plasma. The amount of elongation, κ, is directly proportional to the decay index, giving a relation between elongation and the vertical instablility[18]. The magnitude of S_B determines the speed of vertical instability that has to be controlled. Since the plasma current is conserved in this model, only the n_i term in equation 3.4 changes the variable S_B. The decay index is the variable that is altered to represent a change in the decay index force, F_{DI}.

The conducting vacuum vessel surrounding the plasma supplies the second force on the plasma. As the current contained in the plasma moves, it will induce eddy currents in the vacuum vessel which will resist the plasma motion. This force can be large enough to counter the effects of F_{DI} and provide passive stabilization to the plasma. The ALCATOR C-Mod Tokamak has a highly conductive stainless steel vacuum vessel for just that reason. Passive stabilization only works up to specific value of decay index after which active stabilization using magnetic coils is required[19].

For the purposes of this research, it is assumed that the plasma elongation is such that active stabilization is required. The force term caused by the eddy currents in the vacuum vessel is

$$F_{Eddy} = I_p \sum_i^{NC} \frac{\partial M_{PCi}}{\partial z} I_{Ci} \equiv \hat{S}_C \hat{I}_C \qquad \textbf{3.7}$$

where F_{Eddy} is the force provided by the vacuum vessel, M_{PCi} is the mutual inductance between the plasma and the i'th conducting filament, and I_{ci} is the current in that filament. $\hat{S}_C$ is a vector that allows F_{Eddy} to be expressed as a set of constants multiplied by the currents. Equation 3.2 can now be written as

$$m\ddot{z} = F_{DI} + F_{Eddy} = \hat{S}_C \hat{I}_C + S_B z \qquad \textbf{3.8}$$

The mass of the plasma is small. So if force-imbalance existed acceleration would be very rapid. We therefore assume that the acceleration term can be ignored and the approximate force-balance is always satisfied. This changes equation 3.8 to an equilibrium condition where

$$0 = \hat{S}_C \hat{I}_C + S_B z \qquad \textbf{3.9}$$

This equation can be combined with a model of the currents, $\hat{I}_C$, to fully describe the vertical displacement of the plasma.

3.3 THE CIRCUIT EQUATIONS

The circuit equation is derived from loop voltage equations of all current carrying elements in the model. It is written as

$$\sum_{j}^{NC} \mathbf{M}_{ij} \frac{dI_{Cj}}{dt} + r_i I_i + I_p \frac{\partial M_{PCi}}{\partial z} \frac{\partial z}{\partial t} = V_i \qquad \textbf{3.10}$$

where **M** is the mutual inductance matrix, I_{Ci} is the current in conductor I, r_j is the resistance in conductor I, and V_i is the voltage applied to the conducting element. If the conductor is one of the magnet coils, then the applied voltage can be changed by control laws. Otherwise, the conductor is a passive element where the applied voltage is zero.

If a state vector

$$\hat{x} = \begin{bmatrix} \hat{I}_C \\ z \end{bmatrix} \tag{3.11}$$

is used, then equation 3.10 can be combined with equation 3.9 to create the matrix equation

$$\begin{bmatrix} \mathbf{M} & \hat{S}_C' \\ 0 & 0 \end{bmatrix} \dot{\hat{x}} = \begin{bmatrix} -\mathbf{r} & 0 \\ \hat{S}_C & S_B \end{bmatrix} \hat{x} + \begin{bmatrix} \hat{V} \\ 0 \end{bmatrix} \tag{3.12}$$

where $\hat{S}_C'$, denoting the transpose of $\hat{S}_C$, represents equation 3.10 in terms of equation 3.7. The growth rate of the vertical instability and the conductor currents can be obtained by solving equation 3.12 as a generalized eigenvalue problem of the form

$$\mathbf{A}_1 \hat{x} = \gamma \mathbf{A}_2 \hat{x} \tag{3.13}$$

where $\mathbf{A}_1$ and $\mathbf{A}_2$ contain the circuit and force equations. The growth and damping rates of the filament currents and vertical mode can be easily computed. Control laws can be inserted into the magnetic coil voltages to change the eigenvalue problem and eliminate any growth modes.

The representation described in equation 3.12 fits the first requirement of a model in that it can be easily programmed into a computer. Unfortunately it is not in a form that allows for calculation of control laws using full state feedback (FSFB) gain selection rules. FSFB requires that the model be in state space form,

$$\dot{\hat{x}} = \mathbf{A}\hat{x} + \mathbf{B}\hat{u}, \tag{3.14}$$

where $\hat{u}$ is the input vector. To transform equation 3.12 into state space form, the z position is converted to a vector represented by currents using equation 3.9 and eliminated from the state. The state vector is now represented by the filament currents, $\hat{I}_C$, and the equation becomes

$$\dot{\hat{I}} = \left[\mathbf{M} - \frac{\hat{S}_C' \hat{S}_C}{S_B} \right]^{-1} [-\mathbf{r}] \hat{I} + \left[\mathbf{M} - \frac{\hat{S}_C' \hat{S}_C}{S_B} \right]^{-1} [\hat{b}] \hat{V} \equiv \mathbf{A}_I \hat{I} + \mathbf{B}_I \hat{V} \tag{3.15}$$

where the vertical vector $\vec{b}$ is

$$\begin{aligned} b_i &= 1 \text{ for coil i in series} \\ b_i &= -1 \text{ for coil i in antiseries} \\ b_i &= 0 \text{ for coil i not connected to voltage source} \end{aligned} \qquad \textbf{3.16}$$

While this representation allows for calculation of FSFB gains, it adds the difficulty of determining which mode of the eigenvalue problem represents the vertical motion.

3.4 POWER SUPPLY DYNAMICS

As mentioned in section **1.2**, the dynamics of the power supply are not extensively modeled. It is important, though, to not develop unrealistic control systems. Without any power supply dynamics it is theoretically possible to devise a set of control laws that can stabilize any magnitude of growth rate. The purpose of adding dynamics to this model is to prevent the creation of impossible control systems.

The Chopper power supply contains a capacitor bank hooked up to a series of inductors through a solid state switching system. The capacitor banks are switched on for a length of time determined by the input command, delivering a constant voltage to the circuit. When they are switched off the inductors maintain the current produced. The magnetic coil current sees the average voltage produced during one pulse cycle. The voltage output can change to match an input command over one pulse cycle, which provides the delay in our system.

Since our models are continuous we would like to represent the power supply in the same way. A transfer function formulation is used to provide a rough approximation of the switching time delay. It also has the advantage of easy inclusion in the state space formulation.

The easiest model of the chopper power supply is to consider it as a single pole system. The transfer function,

$$u\frac{\tau}{s+\tau} = V \qquad \textbf{3.17}$$

represents the change in power supply voltage, V, based upon a control signal, u, with τ being the time constant of the system. The response produced is shown in figure 3.2, comparing the state space response to the non-linear response of the chopper power supply. This model works well representing proportional inputs into the system. A problem arose when the single pole model was used with the PD control system. The initial results had the PD system controlling the vertical instability when it had a growth rate twice as fast as the power supply. The reason for this was discovered to be a property of the single pole power supply model. With PD control the transfer function becomes

$$u\frac{(s+\alpha)\frac{\tau}{\alpha}}{s+\tau} = V \qquad \textbf{3.18}$$

where α is a constant of the PD system. Since the acceleration of a single pole system is infinite, the derivative term takes on an instantaneous value without experiencing a delay time. In order to model the chopper power supply delay an a PD system, a second pole had to be added. The transfer function,

$$u\frac{(s+\alpha)\frac{\tau^2}{\alpha}}{(s+\tau)^2} = V \qquad \textbf{3.19}$$

provides a reasonable delay for the derivative term. The proportional and derivative output of this system are shown in figure 3.3, in comparison to the results achieved from a chopper supply. The fit is not ideal, but it does maintain the delay time instituted by the chopper system. Use of the two pole system with the state space control produced instabilities in our model. This is a result of developing the state space model without the power supply dynamics taken into account. The single pole system was retained for state space control, since it provided the delay needed without forcing a new design of a state space control system. Unfortunately this effect cannot be achieved by using the same power supply for both models.

The dynamics can be easily incorporated into state space form by using the state vector

$$\hat{x} = \begin{bmatrix} \hat{I}_C \\ \hat{V} \end{bmatrix} \tag{3.20}$$

with $\hat{V}$ representing the states of the power supply, and the system

$$\dot{\hat{x}} = \begin{bmatrix} \mathbf{A}_I & \mathbf{B}_I \\ 0 & \mathbf{A}_{ps} \end{bmatrix} \hat{x} + \begin{bmatrix} 0 \\ \mathbf{B}_{ps} \end{bmatrix} \hat{u} \tag{3.21}$$

with $\mathbf{A}_{ps}$ and $\mathbf{B}_{ps}$ representing the state space description of the power supply. Once the dynamics are added to the system it is possible to estimate the limits of one control system in comparison to another.

There are several other power supplies, controlling magnetic coils, that do not receive control commands to stabilize the vertical position. They are used to manipulate several properties of the plasma. The assumption is that other power supplies will try to maintain preprogrammed currents. A simple model of the current in an individual power supply is

$$L\dot{I}_C = -rI_C + V \tag{3.22}$$

where L is the circuit inductance. The voltage can be replaced with a negative gain feedback in the form V=-GI, giving us

$$L\dot{I}_C = -(r+G)I_C \qquad \textbf{3.23}$$

This adds to the magnitude of the resistance term, and changes the decay rate of coil currents containing the other power supplies. Added to equation 3.15 produces the model

$$\dot{\hat{I}} = \left[\mathbf{M} - \frac{\hat{S}_C'\hat{S}_C}{S_B}\right]\left[-(\mathbf{r}+\mathbf{G})\right]\hat{I} + \left[\mathbf{M} - \frac{\hat{S}_C'\hat{S}_C}{S_B}\right]\left[\hat{b}\right]\hat{V} \equiv \mathbf{A}_I^*\hat{I} + \mathbf{B}_I\hat{V} \qquad \textbf{3.24}$$

where **G** is a diagonal matrix containing gains for the modeled power supplies and zeros for the passive conductors.

With the completed model derived, the growth rate of the vertical growth mode as a function of the decay index, n_i, was graphed. Figure 3.4 shows the results. The plasma current is set at 2 MA and the vertical field, B_z, is taken to be that required for radial force balance. The equation is

$$B_z = \frac{\mu_o I_p}{2\pi a}\frac{a}{2R_p}\left[\ln\frac{8R_p}{a} - \frac{3}{2} + \frac{\ell_i}{2} + \beta_p\right] \qquad \textbf{3.25}$$

where the plasma minor radius is a=0.21 m, major radius R_p=0.67 m, internal inductance ℓ_i=1, and β_p=0. B_z turns out to be 0.669 Tesla. Figure 3.4 shows the growth mode coming from an asymptote at $n_i \approx$-1.5 and decreasing in speed as n_i becomes less negative. To the left of the asymptote represents a plasma condition that violates MHD equilibrium and cannot be represented by this model. The difficulty in controlling the plasma is represented by the larger positive time constants for the more negative combined index. Figure 3.5 shows the currents

associated with the growth eigenmode. The axisymmetric current distribution about the centerline is responsible for pushing the plasma along the vertical axis.

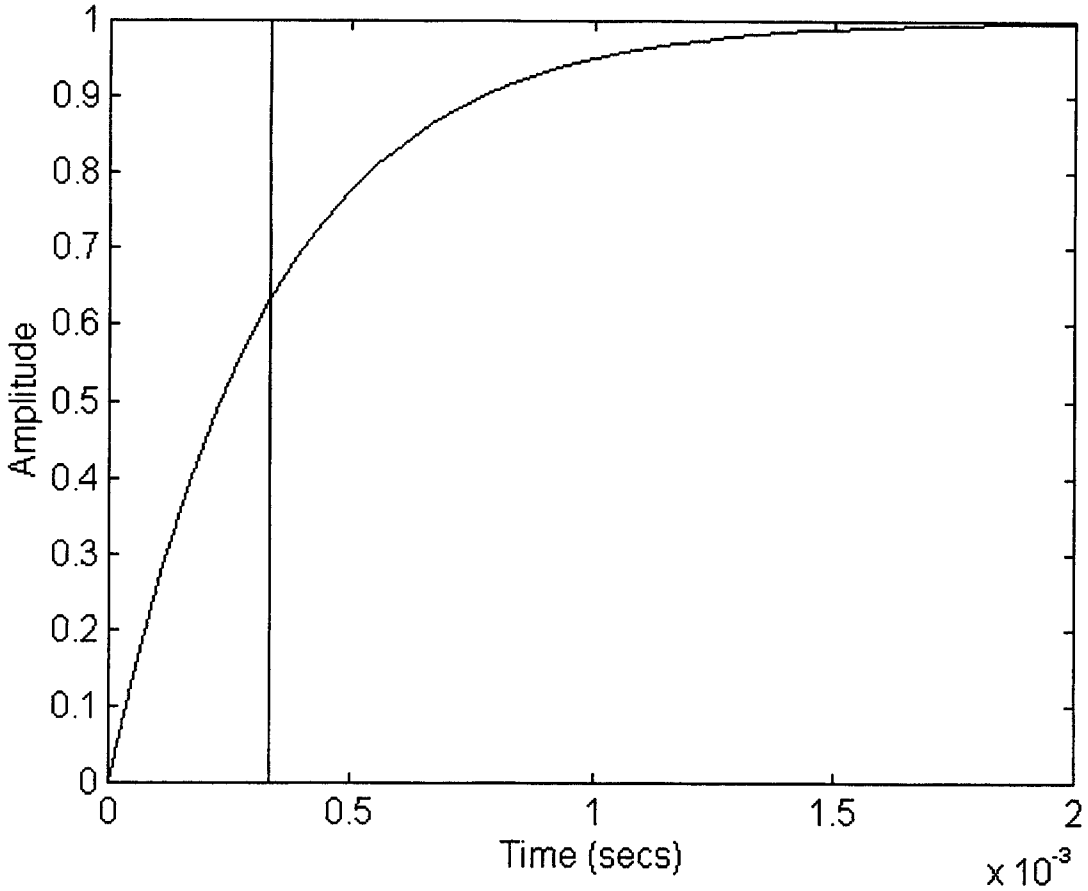

Figure 3.2 The single pole power supply. The stepped response represents the chopper response to an input. This is the most basic representation of the power supply.

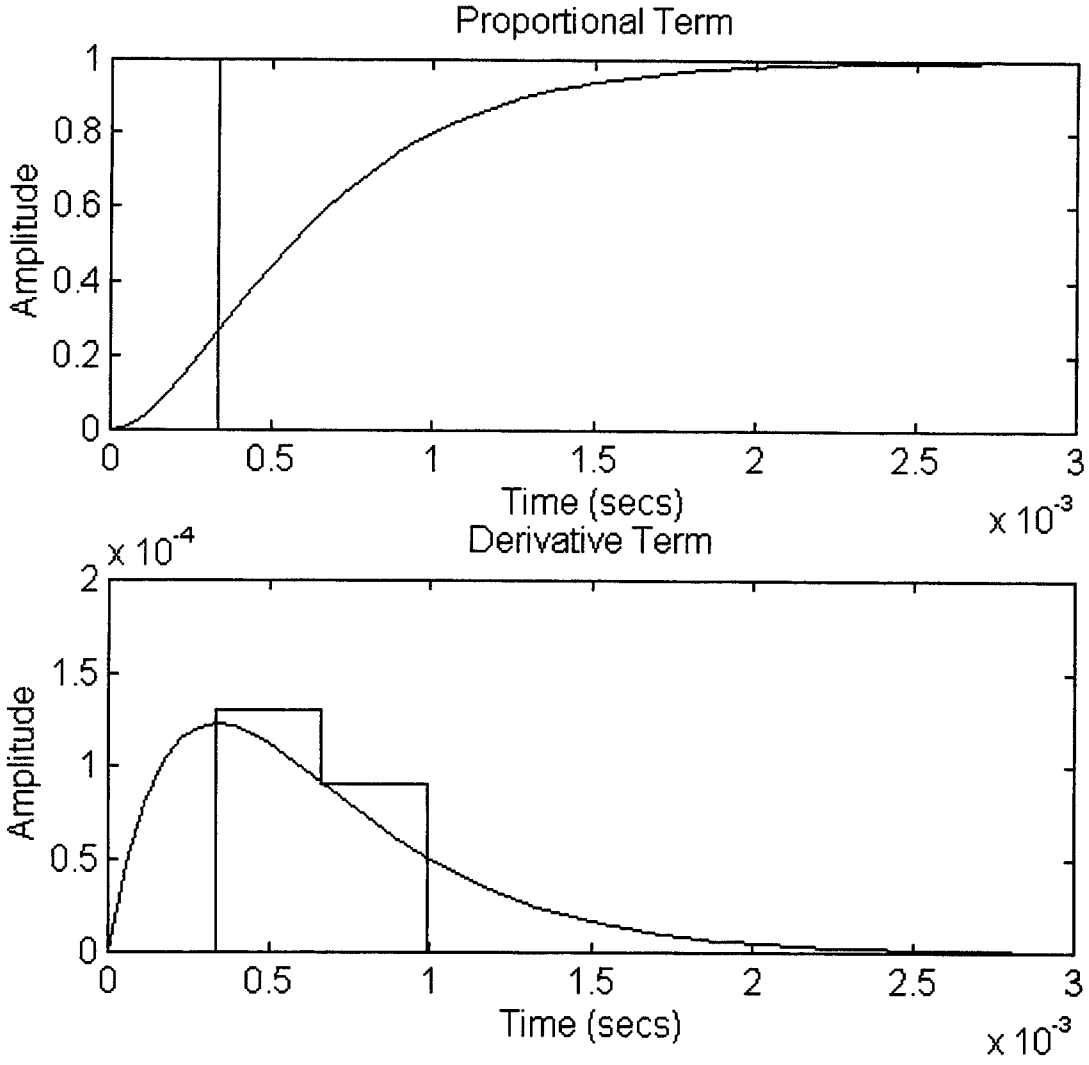

Figure 3.3 The two pole power supply for the PD system. The step response shows how the chopper power supply is supposed to react to inputs in the system.

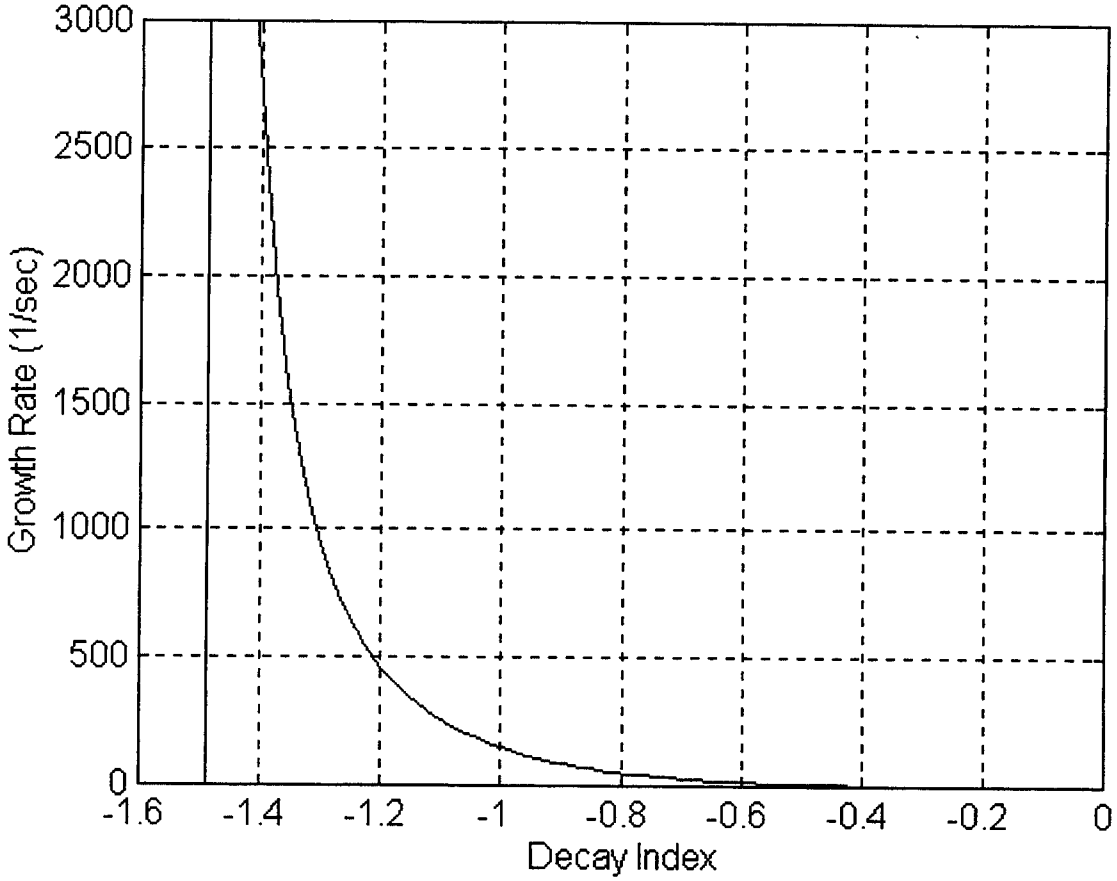

Figure 3.4 Growth rate as a function of n_i. The point where the model fails is noted by the strait line on the left.

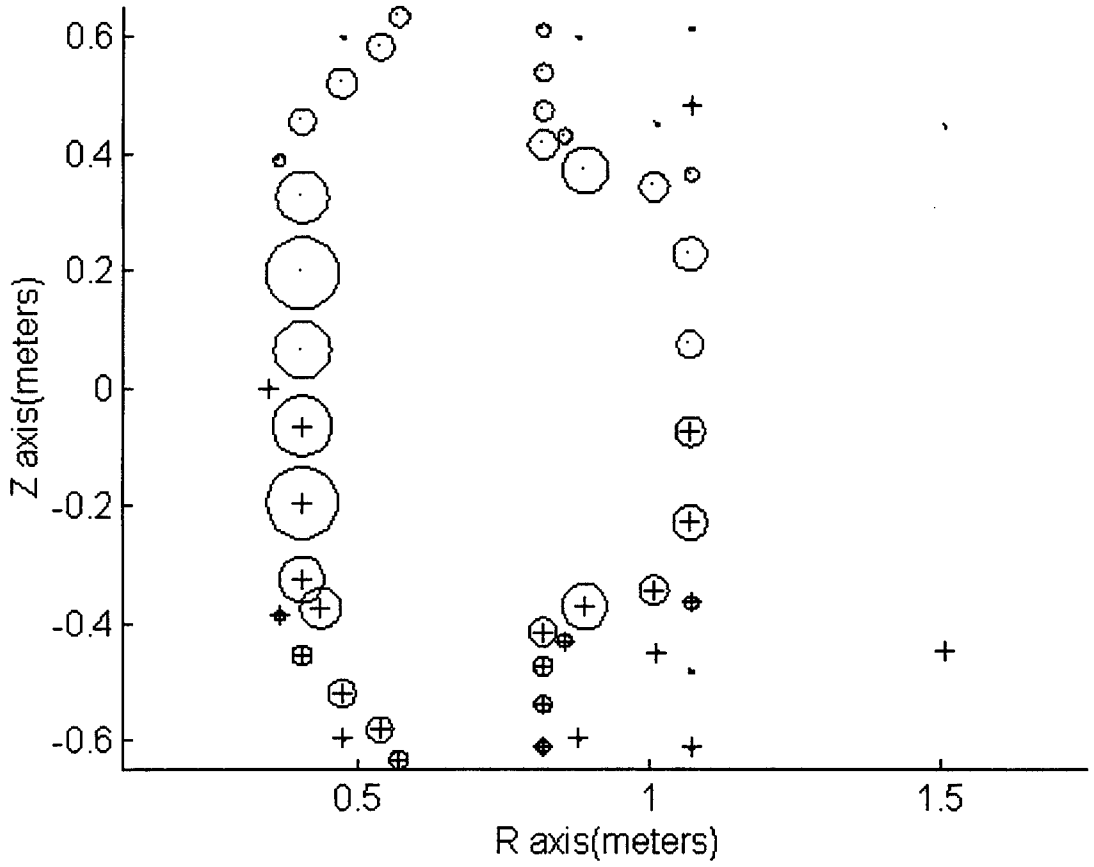

Figure 3.5 This is a plot of the conductor currents associated with a pure growth mode that has a decay index n_i=-1.32 and γ=1067 (1/sec).

CHAPTER 4

CONTROL METHODS

The vertical position of the plasma is stabilized by feedback control. The idea of feedback control is to take an output signal and return it as input through a feedback loop. A simple example is of a person adjusting the water temperature of a faucet. After feeling the water coming out of the faucet(output), the person adjusts the knob(input) to change the temperature of the water. Here, the person comprises the feedback loop that maintains a desired temperature for the water. For the vertical position of the plasma, the feedback loop consists of system measurements, a control computer, and a voltage signal to the chopper power supply.

A list of criteria for identifying feedback systems is given by Mayr[20]. They are:

1. The feedback system maintains a prescribed relationship of one system variable to another, . . . in spite of external disturbances.
2. This is done by comparing functions of these variables and using the difference as a means of control.
3. The system includes a sensing element and a comparator, at least one of which can be distinguished as a physically separate element.

The two feedback systems compared are PID control and FSFB control. The differences between these systems can be described by the ways that they fulfill specific parts of these conditions. A listing is given in the sections on each control method.

Other than the type of feedback system used, two different coil and plasma models are considered. In the first model, the plasma position is controlled by the EFC coils. This corresponds to a specific $\vec{b}$ vector in the system model described by equation 3.16. In the second system, the $\vec{b}$ vector represents control input through the OH2 coils. Both a PID and FSFB control was developed and compared for each coil and plasma model. Using the two separate feedback systems with the two control system methods gives us four separate cases to compare. The analysis of these cases is covered in chapter 5.

4.1 PID CONTROL

Using Mayr's criteria, the PID system for our system can be described as follows:

1. PID uses the relationship between the actual z position and the desired z position of the plasma.
2. The comparison between the actual position and desired position is defined as $\tilde{z} \equiv z - z_0$, where z_0 is the desired position of the plasma. This difference is returned into the voltage commands by means of a control signal, u, using the following function

$$u = P\tilde{z}(t) + I\int_0^t \tilde{z}(t)dt + D\frac{d\tilde{z}(t)}{dt} \qquad \textbf{4.1}$$

where P is the proportional gain, I is the integral gain, and D is the derivative gain.

3. The sensing element is required to measure the position of the plasma. Since our desired position of the plasma z_0=0, the sensing element performs the function of the comparator by returning z=$\tilde{z}$.

The PID controller can provide robust performance in a wide range of operating conditions[7]. A form of the PID controller is used currently to control plasma vertical position in the ALCATOR C-Mod tokamak.

To use equation 4.1, the three gains, P, I, and D, must be determined for a given process[21]. The larger the P term, the swifter the control system response is to a change in plasma position. This increases the speed with which the plasma returns to position. The I term is used to remove steady state error, which is the value of $\tilde{z}$ when the time period is large and the transient response of the system has decayed. Most systems with only a P gain have this characteristic. The I term will slow the speed of the control system response, and move the system toward an unstable dynamic. The D term adds damping to the control response. This reduces the overshoot and settling time of the system. Overshoot is the amount the plasma position moves beyond the desired position in response to the control system command. Settling time refers to the time it takes for the position output to settle within a certain range of the desired position[7]. The last two conditions are sometimes increased by a larger P term. The various terms of a PID controller can be tailored to produce most desired responses for a system.

4.2 ROOT LOCUS GAIN SELECTION

The PID gains were determined for this system by root locus analysis. Root locus graphs show a change in the eigenmode values of the system with respect to a change in a gain

variable. The coordinates and details of the graph are given in figure 4.1. The vertical axis corresponds to the imaginary value of a system eigenmode and the horizontal axis corresponds to the real value. The values on the right side of the imaginary axis are unstable, and correspond to the growth mode of a system. It is desired to move all eigenmodes from the right hand side of the root locus graph to the left hand side. Position of an eigenmode on the graph relates to its time dependent behavior. For our purposes we are concerned about two properties. The amount of damping of a variable is described by a dimensionless damping ratio ζ, which is equal to the cosine of angle α. When $\zeta=1$, the oscillation term of the time solution is removed and the system is critically damped[7]. Any values less than one describe an under damped system. The inverse of distance A is approximately four times the settling time of a state variable.

Optimization for a PID system can be described in terms of a performance index, the integral of time multiplied by absolute error(ITAE). The form of the index is

$$\text{ITAE} = \int_0^T t|e(t)|dt \tag{4.2}$$

with *e(t)* representing the error between the actual and desired position of a system[7]. This index reduces emphasis upon the initial error of the system, and concentrates more on future performance. The analytical solution of the ITAE is very difficult for our 50 order system, so a two order system approximation was used as a starting design point. In a two order system, the ITAE is minimized when the damping ratio $\zeta \approx 0.7$ [7]. This corresponds to an $\alpha=45°$ on the root locus graph.

To determine the PID gains for our control system, different values were set for two of the gains while a third one was varied. The initial results showed that the I term added an

unstable eigenmode to the system, so it was eliminated. A PID system with the I term removed is called a proportional-derivative (PD) controller. The next series of root locus graphs set a ratio between the P and D variables at a constant, and swept the overall gain of the system. By setting this ratio at a set value, the trace of the root locus poles traced out a near circular path around the stable point. This path allowed for easy selection of the pole's optimum position as determined by the ITAE index. The ratio P/D has units of (1/sec), and on our root locus graphs it is proportional to the diameter of the circular path traced by the poles. This path can be made to reach a set value of A, with the optimum ζ determining the P and D values. The A value was chosen by borrowing from the eigenmode performance of the FSFB system, so that excessive performance from unusably large gains was avoided. A root locus graph that would place the poles at a desired point was created for both the PD and EFC system. Figures 4.2 and 4.3 shows the root locus graph and discuss the values chosen in the design.

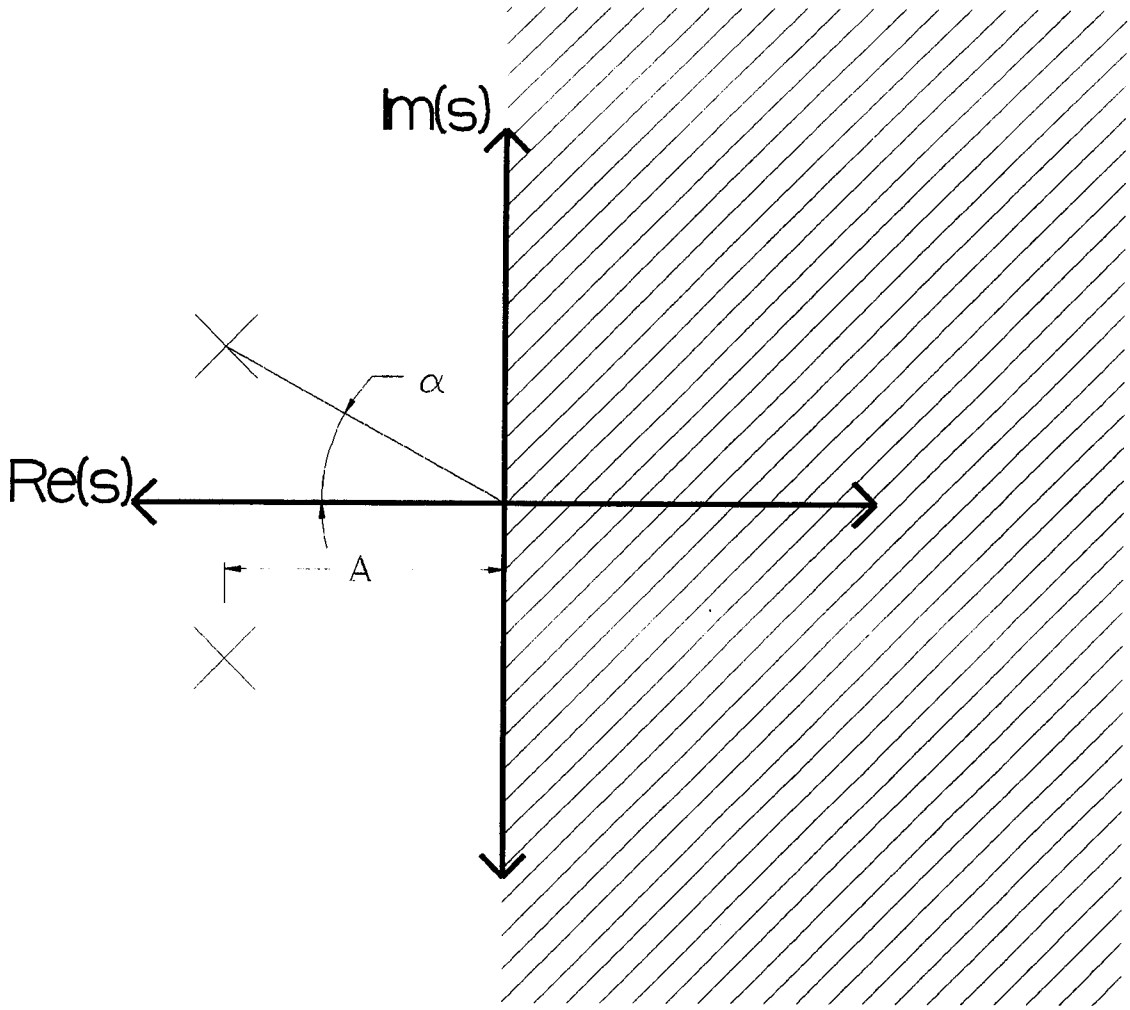

Figure 4.1 Figure showing the geometry of the root locus graph. All points on the right side of the imaginary axis are unstable.

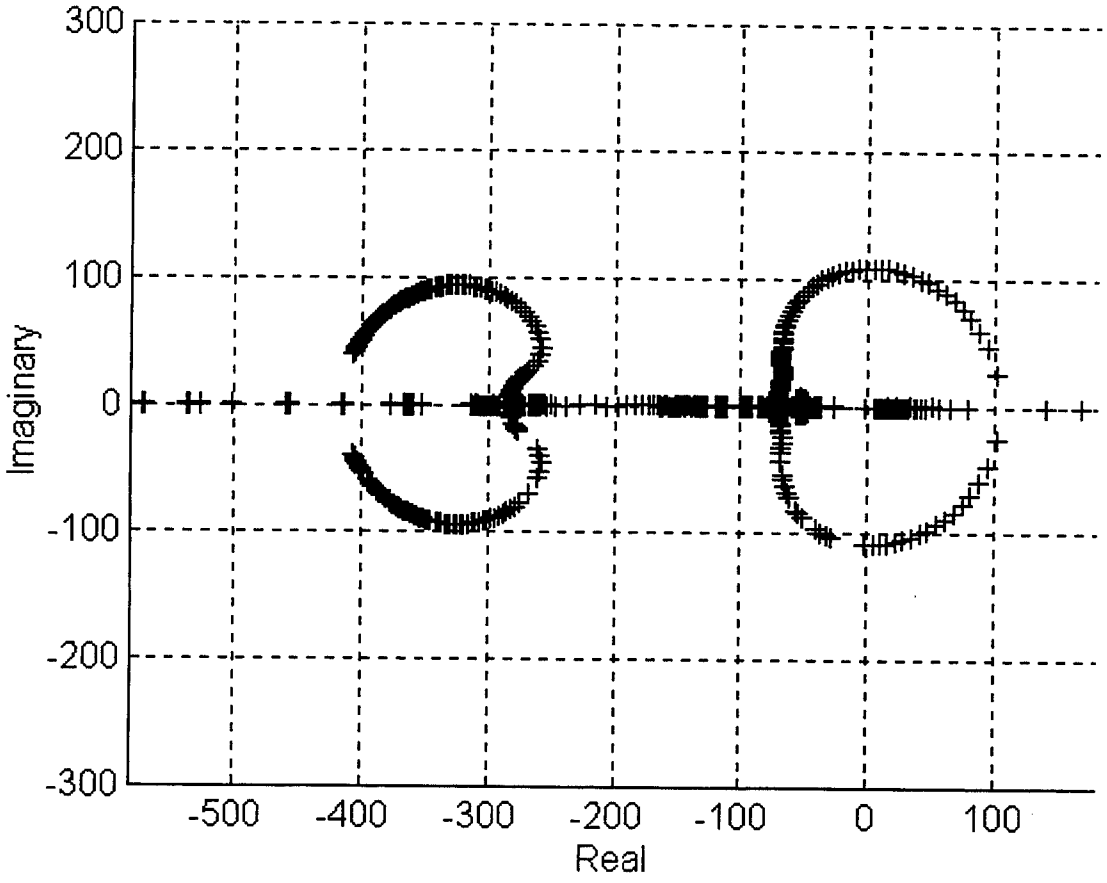

Figure 4.2 Root locus graph of EFC PD control system, with the rightmost trace describing the change of the uncontrolled growth mode(γ=1065 (1/sec)). The PD ratio for this graph is set at 33.3 (1/sec). For α=45° and A≈65 (1/sec), the gain values are P=2510 (V/m) and D=75 (V·sec/m).

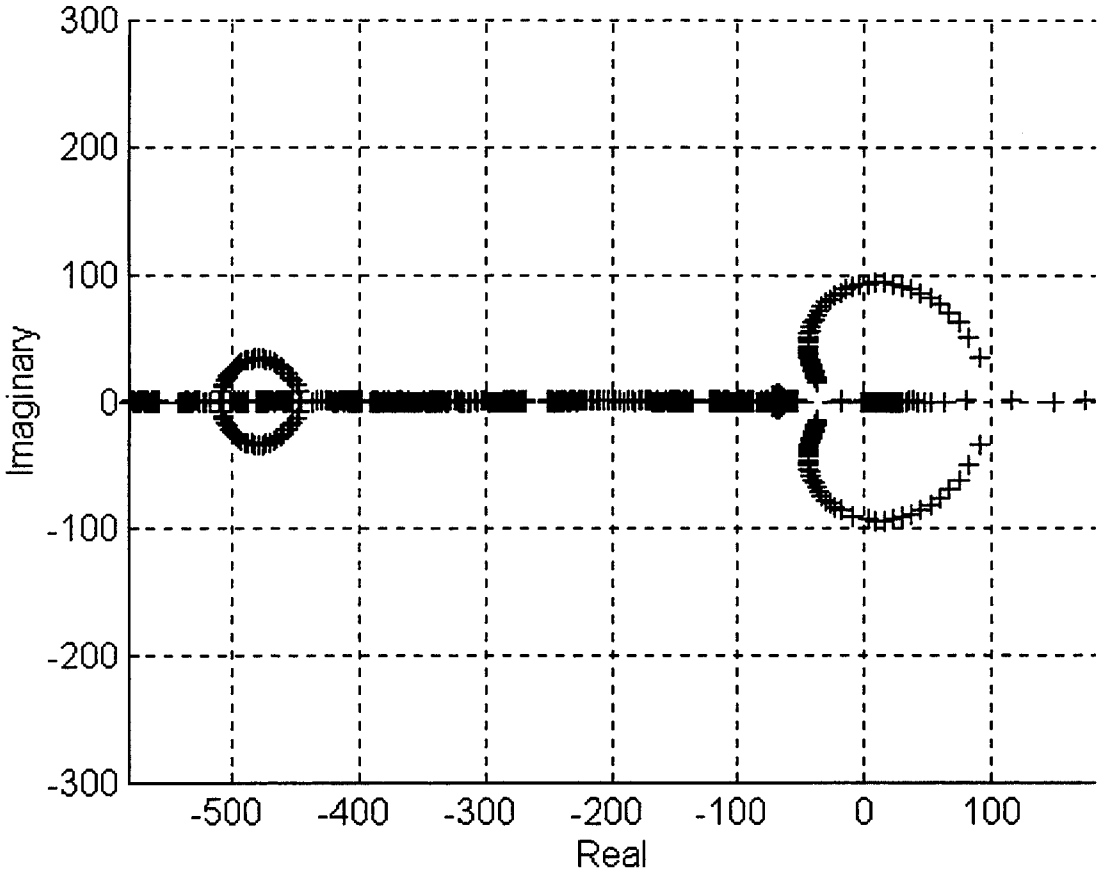

Figure 4.3 Root locus graph of OH2 PD control system, with the rightmost trace starting in the same position as figure 4.2. The values for the graph design point are the same as the EFC control with P/D=33.3 (1/sec), α=45°, P=2510 (V/m) and D=75 (V·sec/m). The distance on the real axis was A=46 (1/sec).

4.3 FSFB CONTROL

The Mayr criteria for Full State feedback are:

1. FSFB uses the relationship between all of the states of the system, $\hat{x}$, and the desired z position of the plasma.

2. The comparison is between a linear function relating the states to the vertical position z and the desired position of the plasma. The linear function for the z position is

$$z = \mathbf{C}\hat{x} \tag{4.3}$$

where the matrix **C** transforms the states to the z position of the plasma. This is controlled by feeding back a signal, $\hat{u}$, to the input, where

$$\hat{u} = -\mathbf{K}\hat{x} \tag{4.4}$$

with **K** as a matrix of gains.

3. The sensing element needs to give the state vector, $\hat{x}$, to the control system. Sometimes this is impractical or impossible, depending upon the states to be measured. In that case, FSFB requires an estimator to predict the states of the system.

When equation 4.3 is placed into the state space form given by equation 3.14, it changes the system to

$$\dot{\hat{x}} = (\mathbf{A} - \mathbf{BK})\hat{x} \tag{4.5}$$

FSFB can thus radically alter the eigenvalue problem. If the condition for controllability is met, namely that the rank of the matrix $\begin{bmatrix}\mathbf{B} & \mathbf{AB} & \dots & \mathbf{A}^{i-1}\mathbf{B}\end{bmatrix}$ is equal to i, with i equal to the number of states, then all of the eigenmodes of the system can be altered at will[22,23].

The proper selection of the **K** matrix can control the dynamics of the system, including response time, settling time, and damping[23]. It also has the advantage that several types of gain selection methods can be used to optimize the system for specific types of performance. Even if the condition for controllability is not met for all of the states in our system, producing a stable system is still possible if the unstable states are controllable.

4.4 LINEAR QUADRATIC REGULATOR PROBLEM

The gain matrix, **K** , for our FSFB controller was determined by solving the Linear Quadratic Regulator (LQR) problem. This method automatically provides a stable system with guaranteed levels of stability robustness[24]. The LQR problem is posed as follows. For a state space system,

$$\dot{\hat{x}} = \mathbf{A}\hat{x} + \mathbf{B}\hat{u} \tag{4.6}$$

with $\hat{x}(0)=\hat{x}_0$, determine a control $\hat{u}$ such that the quantity

$$J(\hat{x}_0, \hat{u}, t) \equiv \int_0^t \left(\hat{x}'\mathbf{Q}\hat{x} + 2\hat{u}'\mathbf{S}\hat{x} + \hat{u}'\mathbf{R}\hat{u}\right)dt \tag{4.7}$$

is minimized[25]. The matrices **Q** and **R** are weighting matrices that determine the importance of minimizing specific states and inputs. The matrix **S** is used to add damping to the closed loop response. Both **Q** and **R** ≥ 0, with the matrix $\begin{bmatrix}\mathbf{Q} & \mathbf{S} \\ \mathbf{S}' & \mathbf{R}\end{bmatrix} \geq 0$.

Considering the input, û, represented by equation 4.3, we need to discover the values in the gain matrix, **K**, that will minimize equation 4.6. If the unstable states are controllable, then the values for **K** are [25]

$$\mathbf{K} = \mathbf{R}^{-1}(\mathbf{S}' + \mathbf{B}'\mathbf{N}) \tag{4.8}$$

with **N** being the solution to the algebraic Riccati equation

$$\mathbf{N}\mathbf{A}_n + \mathbf{A}_n'\mathbf{N} + \left(\mathbf{Q} - \mathbf{S}\mathbf{R}^{-1}\mathbf{S}'\right) - \mathbf{N}\mathbf{B}\mathbf{R}^{-1}\mathbf{B}'\mathbf{N} = 0 \tag{4.9}$$

with

$$\mathbf{A}_n = \left(\mathbf{A} - \mathbf{B}\mathbf{R}^{-1}\mathbf{S}'\right) \tag{4.10}$$

The solution to this equation was done numerically through a Matlab Systems Toolbox program.

For the ordering of our system, **Q** is (50x50), **S** is (1x50), and **R** is (1x1). The **K** matrix produced for our single input system has dimensions of (1x50). The choice of **Q**, **S**, and **R**, matrices was determined by experimentation with several initial values. The desired performance was for the fastest possible control of the growth mode after power system dynamics were added. For the first analysis **Q** was a (50x50) identity matrix, **S** was left as a null matrix, and **R** was scaled up and down from a value of 1 to test the effects of minimizing the input. The **K** matrices produced all had the same eigenmode performance, meaning that the LQR solution minimized the input of this system for any **R** scaling. The damping of the system turned out to be excellent without the **S** matrix, so it was ignored for further calculations. The next optimization examined had the diagonal of **Q** replaced with the values of $\hat{S}_C$, in an effort to minimize the z position with respect to the currents in equation 3.9. The **K** values produced did not change the performance of the initial gain calculation by any appreciable margin. The best results from the optimization method came from changing the state space system used. The first

analysis values of **Q** and **R** were used, and the decay index of the model was varied. The **K** matrix produced was optimized for the fastest possible control. Figures 4.4 and 4.5 show a graphical representation of the developed gains for the EFC and OH2 control systems respectively. The relative magnitude and direction of the developed **K** matrix are plotted against the current filaments that serve as inputs into the control equation.

4.5 ESTIMATOR OPTIONS

A major problem with using FSFB is the need to know the real time performance of the states. In some systems the states can be directly measured with sensors and fed into the **K** matrix. For our case, 37 of our modes are currents in the vacuum vessel that are inaccessible for gain calculation. In order to use these modes as part of the control system a state estimator is created that can determine unknown states. There are several ways to do this and they can all be divided into two categories, a computer model of the state space system or a linear transformation of indirect measurements. The computer model of the state space system, which follows the form in equation 3.14, can take the input and output signals of a FSFB control system and produce a robust and noise resistant estimate of unknown states. The problem with this system is the computational power needed to perform integrations on 50 states within a real time framework. The ALCATOR C-Mod control computer only has 16 integrators available, and these will not be adequate for our estimation needs.

The linear transformation of indirect measurements will operate with our current control configuration. This type of estimator has the form

$$\hat{x} = \text{pinv}(\mathbf{C})\hat{y} \qquad \textbf{4.11}$$

where $\hat{y}$ is the output of measurements in the system and **C** is a linear transformation that maps the state vector, $\hat{x}$, to the output. The pinv function is the pseudoinverse, or generalized inverse, and is an application of singular value decomposition (SVD) of the matrix[22]. The system on the tokamak takes flux measurements and poloidal B-field measurements at 26 positions on the vacuum vessel, giving 52 measurements available for prediction. This allows an exact estimation of the state vector, $\hat{x}$, to be determined from the measurements.

One problem with this arrangement is that the output vector has a level of uncertainty that will effect the prediction of the state vector. One way to examine the resistance to uncertainty is to examine the singular values of the **C** matrix. The singular values correspond to the gains of the linear transformation, and the ratio between the smallest and largest singular value defines the minimum tolerance needed for the measurements. A logarithmic plot of the singular values of the **C** matrix is included in figure 4.6. This graph shows a seven order of magnitude difference between the largest and smallest singular value, which places an unrealistic tolerance on the measurements. This means that it is impossible to measure all the states with our linear combination without producing debilitating errors. With an achievable tolerance of ±0.5%, 14 states can be measured by the linear transformation estimator. This limits the control utility of this estimator for FSFB control. Further investigation into other estimator designs that can overcome the noise problem is left for further examination.

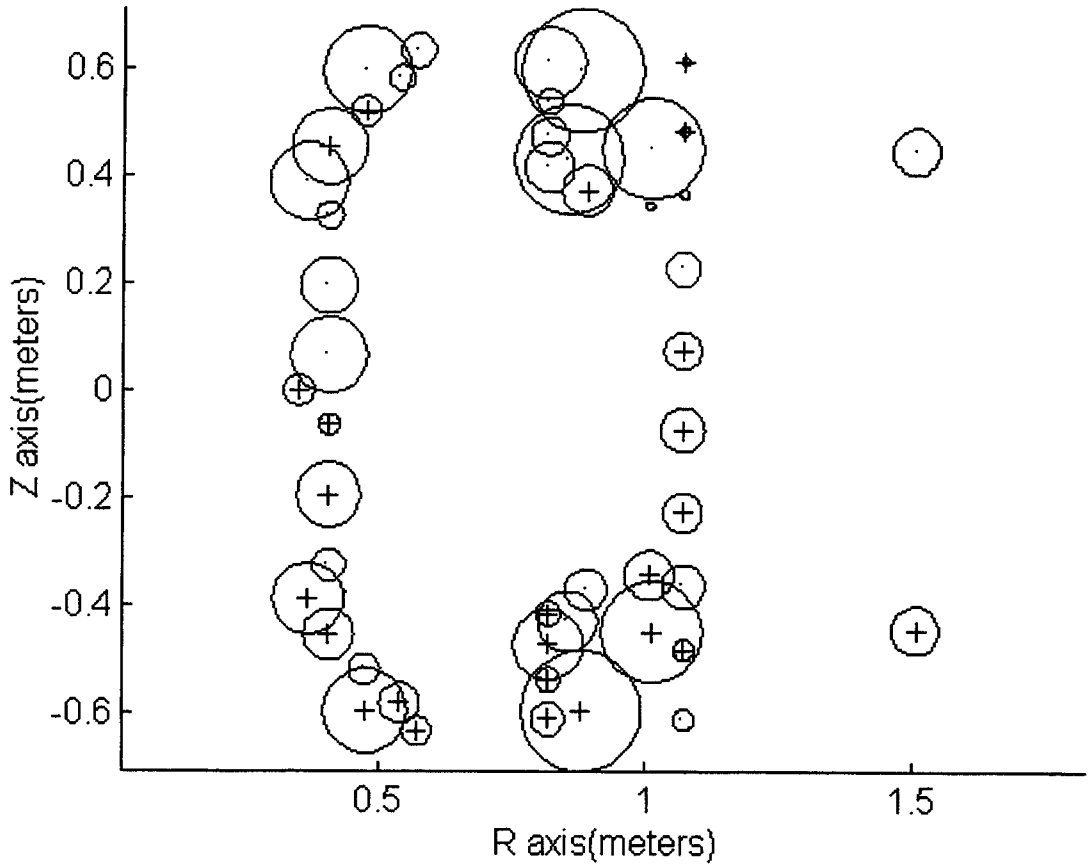

Figure 4.4 Plot of K matrix for EFC control system optimized at n_i=-1.17. The circle area represents a normalized size of the gain value, with a + or · showing the direction of the gain.

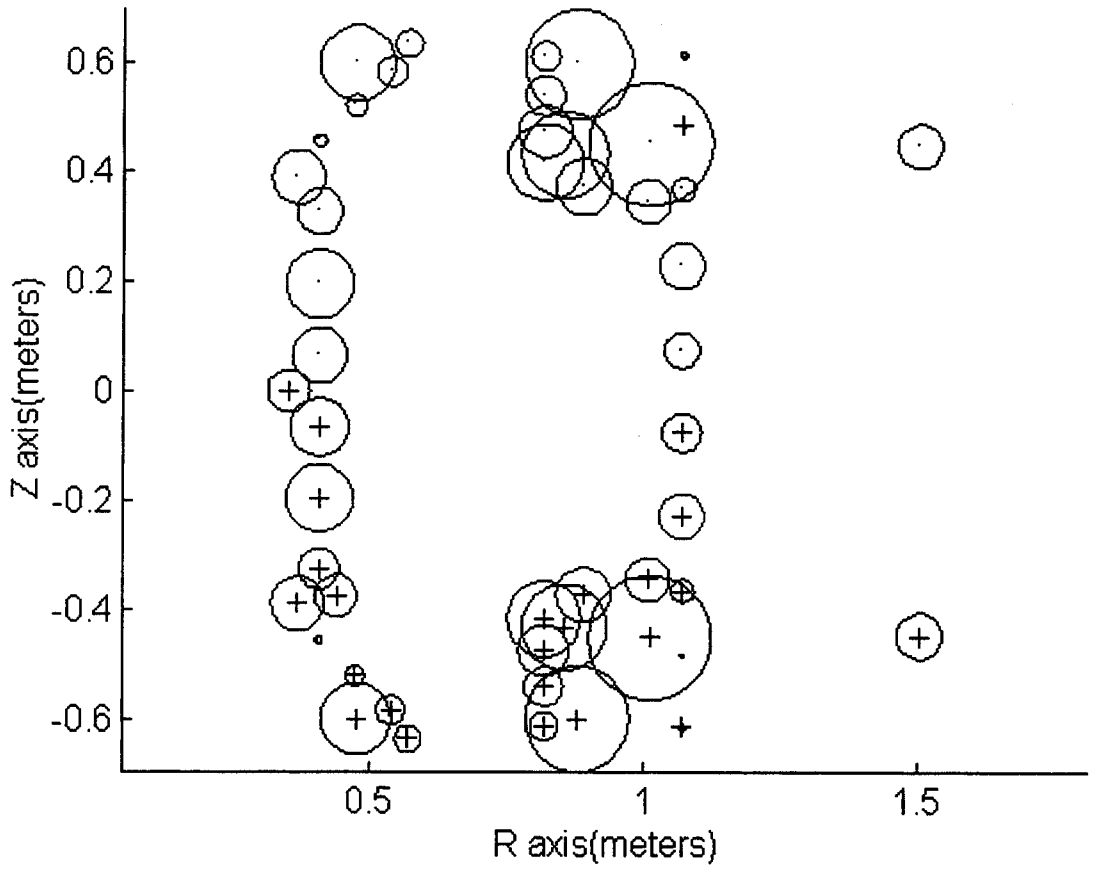

Figure 4.5 Plot of K matrix for OH2 control system optimized at n_i=-1.47. The gain size is normalized with respect to the EFC coils. The difference of the OH2 system can be best seen in the upper outboard coils.

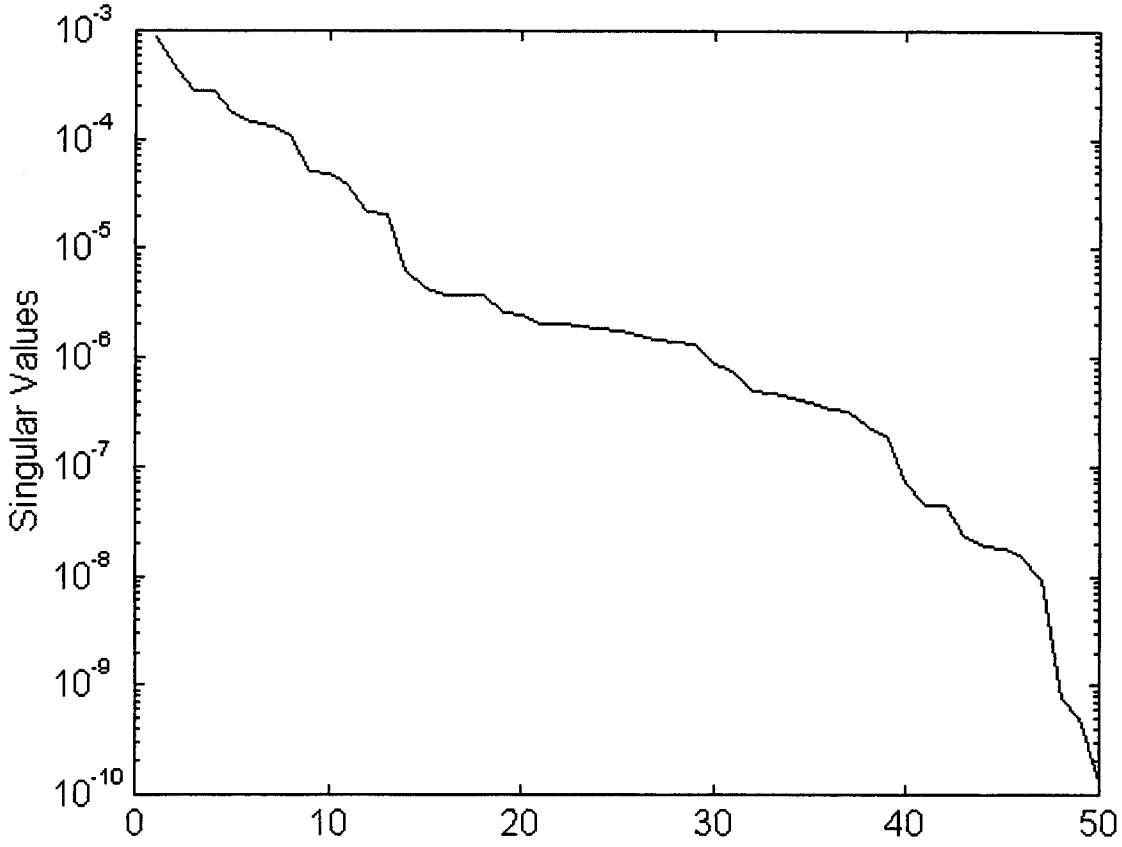

Figure 4.6 Plot of the singular values of the observer matrix C. This graph shows that only 14 states can be determined by the linear transformation with a 0.5% error tolerance.

CHAPTER 5

COMPARISONS AND ANALYSIS

The comparisons of the control systems are based upon two methods, eigenmode analysis and time domain analysis. The eigenmode analysis examines the eigenmodes and vectors of a control model, while the time domain examines the time evolution of a perturbed z value. In combination these two methods can give us basic performance results. The purpose of the analysis is to determine the operating range of the control systems and their performance in that range.

5.1 ANALYSIS METHODS

The operating range is determined by using eigenmode analysis of the system. The number of filaments in our model provides 50 eigenmodes to examine. Most of these modes represent current decay times, while only a few affect the z position of the plasma. To measure the effect of a mode on the z position, a normalized growth moment(NGM) was developed that uses the state information contained in the eigenvector associated with the mode. The representation, derived from equation 3.9,

$$NGM = \frac{\frac{\hat{S}_C}{S_B}}{\text{Constant}} \hat{I} \qquad 5.1$$

70takes the currents of a mode and produces a numerical value that can be compared between modes. The constant was chosen so the NGM of the uncontrolled growth mode in figure 3.5 is 100. Any mode that has a NGM near that value will have an effect on the time performance of the vertical plasma position. The NGM values between growth modes and current decay modes are separated by 2 orders of magnitude, allowing for easy identification. The currents of one of the controlled growth modes is shown in figure 5.1.

The range of system operation was determined by the slowest growth mode in the system. This mode is an approximate indication of the time it takes for the control device to correct a perturbation in the z direction. If the mode falls below 10 (1/sec) then the control system is considered to take too long to correct a perturbation. The second limit occurs as the uncontrolled growth rate gets faster. At one point, the power supply loses the ability to stabilize the system. When this occurs there is a drastic shift of the growth mode from negative to positive.

Due to the large number of states in the system, the range of system operation was limited to a perturbation of the n_i variable. This gives us a single value which is the most important in determining the uncontrolled growth rate. Variations in the other constants of the model were not examined. There are separate issues of robustness that deal with inaccuracies in the **M**, **r**, and $\hat{S}_C$ values of the model. These were not examined due to the large number of variables associated with perturbing these values(2600).

The operating performance of a control system was determined by examining the time domain performance of the system. Since there were several modes that had large NGM values, the one mode does not completely describe the response of the system. An initial displacement

value of z=1cm was set in the model and examined over a time interval. There are three characteristics that this study uses for the time domain analysis. The time it takes for the plasma position to settle within 2% of the position z=0 cm after the initial disturbance is the settling time, T_s. The rise time, T_r, is how long it takes for the plasma position to reach 90% of its desired value. The last value is the percentage of the initial disturbance that the plasma overshoots the desired position. This is referred to by the variable O_S. These values are shown in figure 5.2

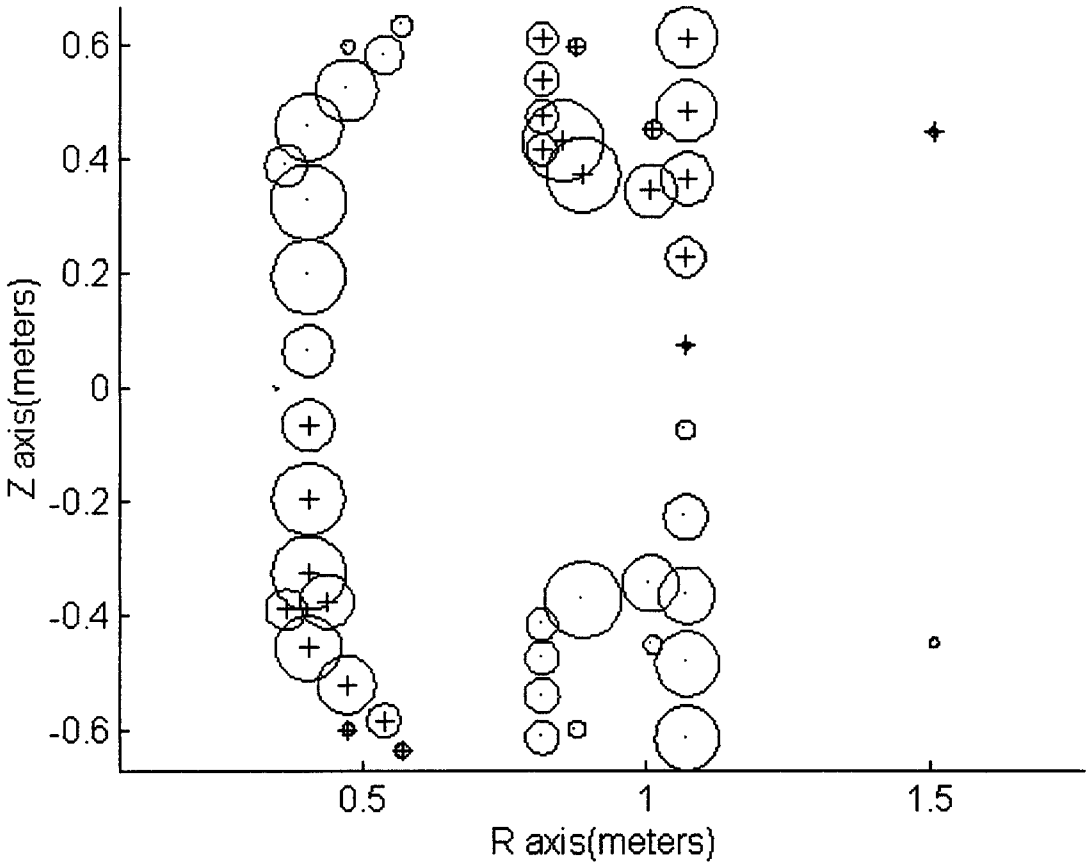

Figure 5.1 Currents associated with an EFC growth mode with a time constant of -35 (1/sec). It has a NGM=110, having a large impact on the z position of the plasma.

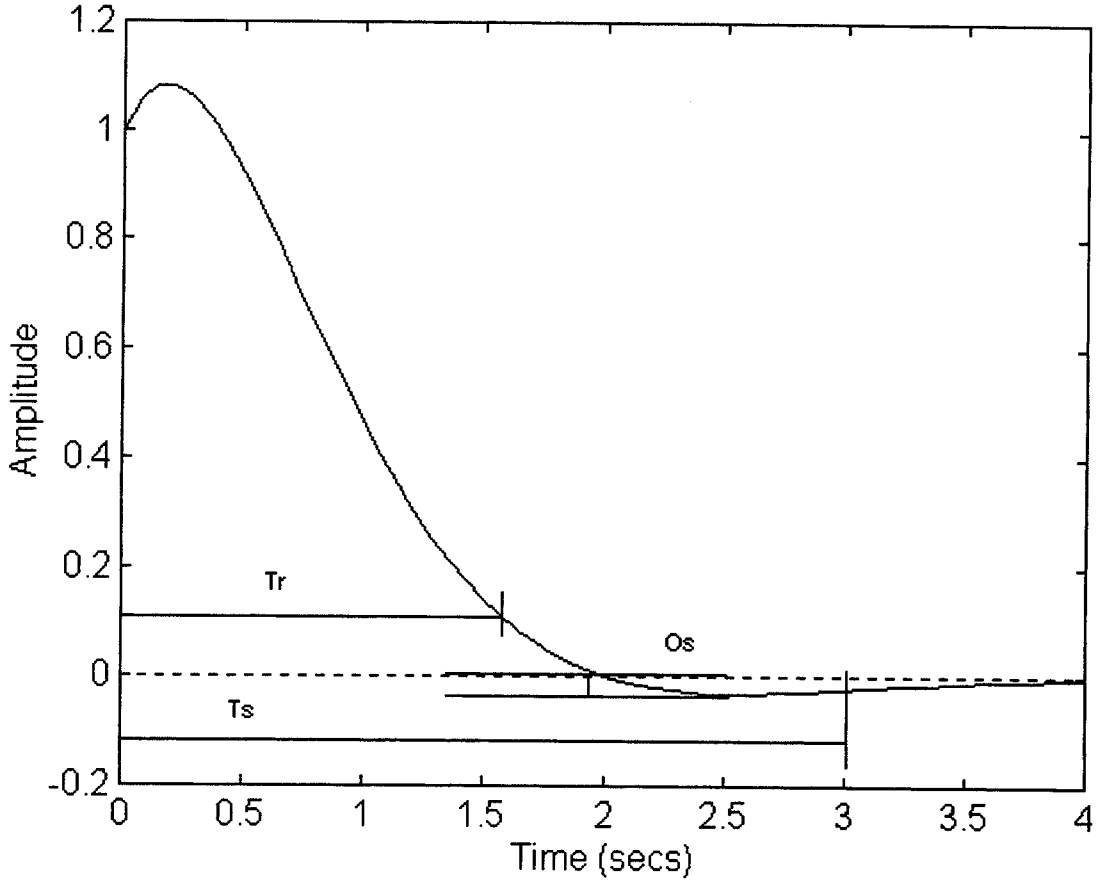

Figure 5.2 Description of characteristics used in time domain analysis.

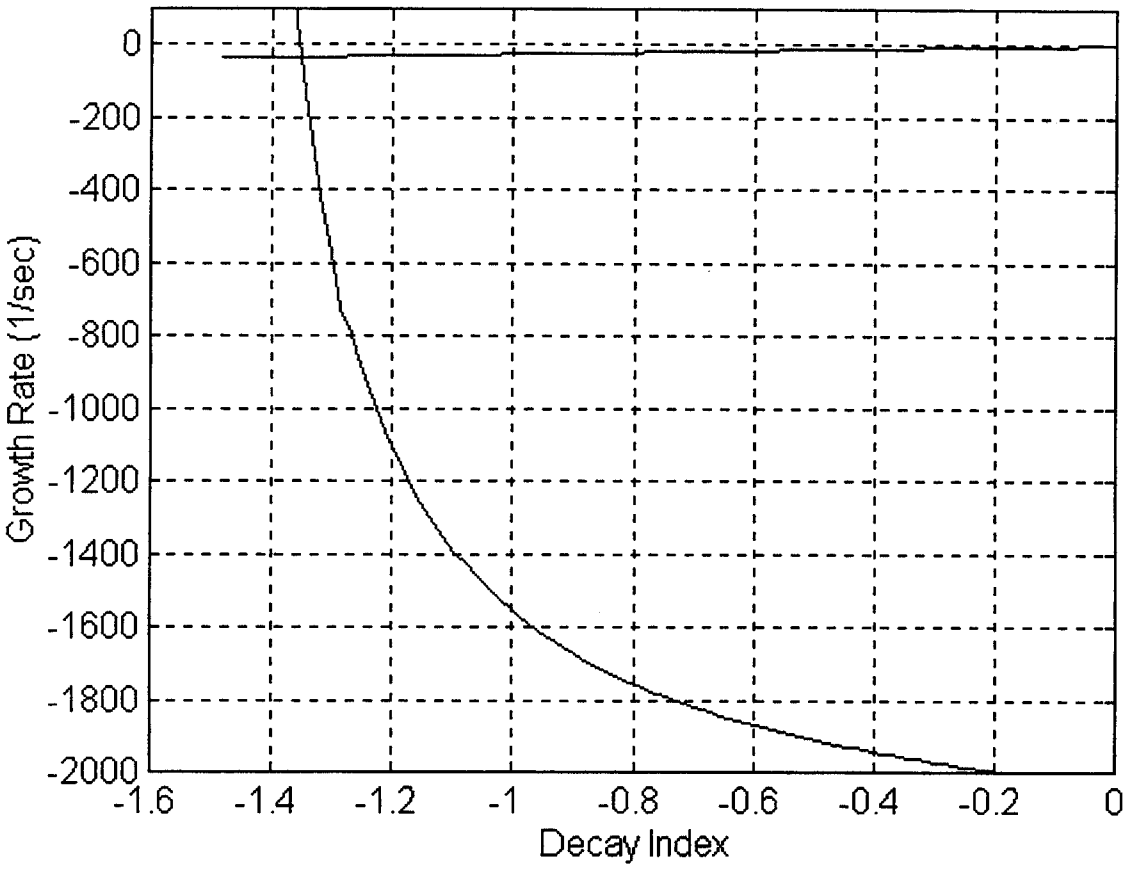

Figure 5.3 Plot of two growth modes as a function of decay index. The slower growth mode dominates the time response, but the second mode determines the point of instability. All robustness plots show the slowest growth mode, with a discontinuity on the graph when the second mode goes positive.

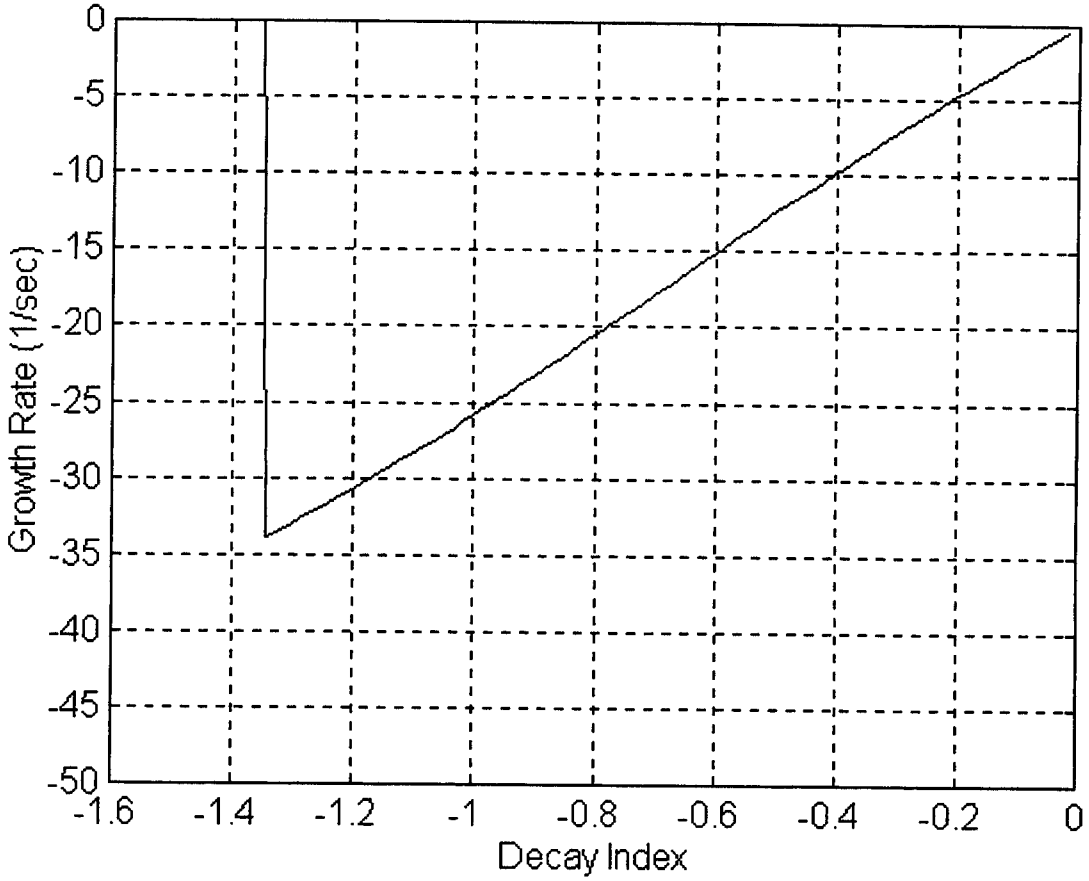

Figure 5.4 Robustness graph for EFC FSFB. The limits of robustness are defined by the mode crossover at n_i=-1.357 and the growth rate becoming slower than -10 (1/sec) at n_i=-0.40. This system had a K matrix optimized for a decay index n_i=-1.18

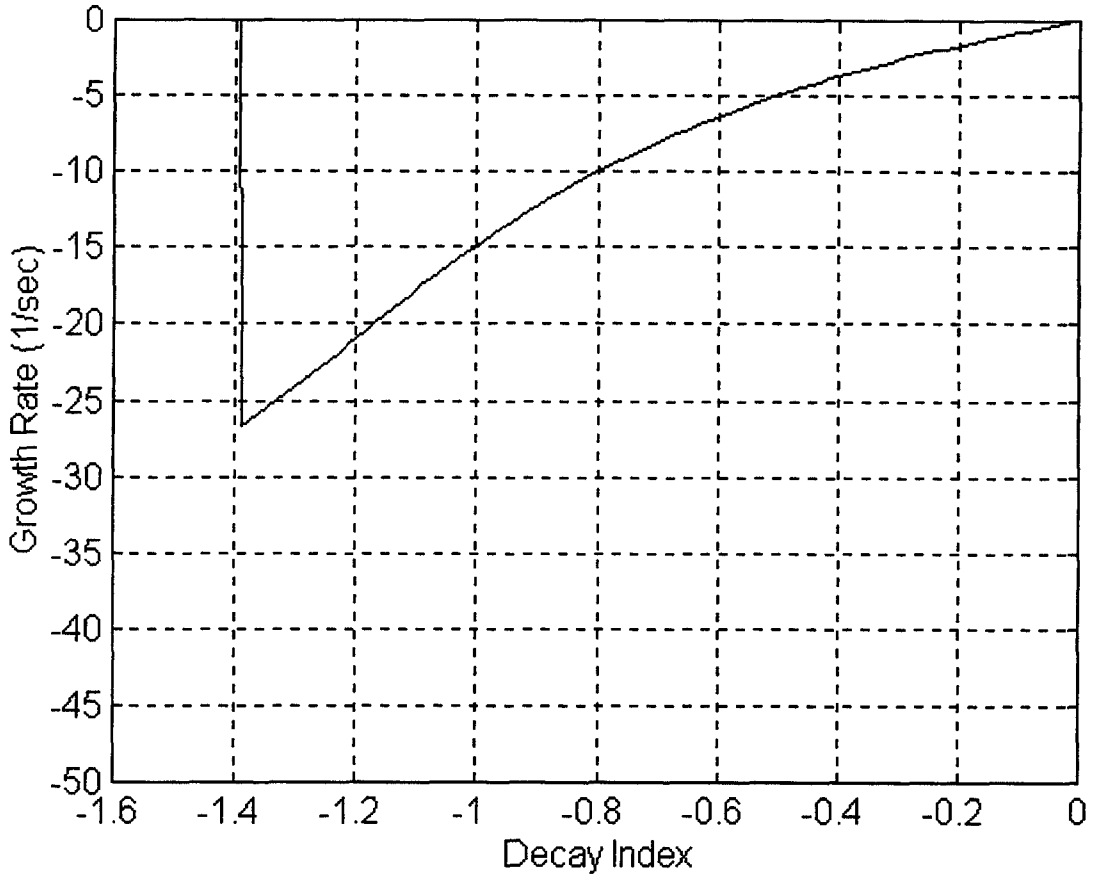

Figure 5.5 Robustness Graph for OH2 FSFB system. This system had a K matrix optimized for a decay index of n_i=-1.47, which was a stable point before the addition of power supply dynamics.

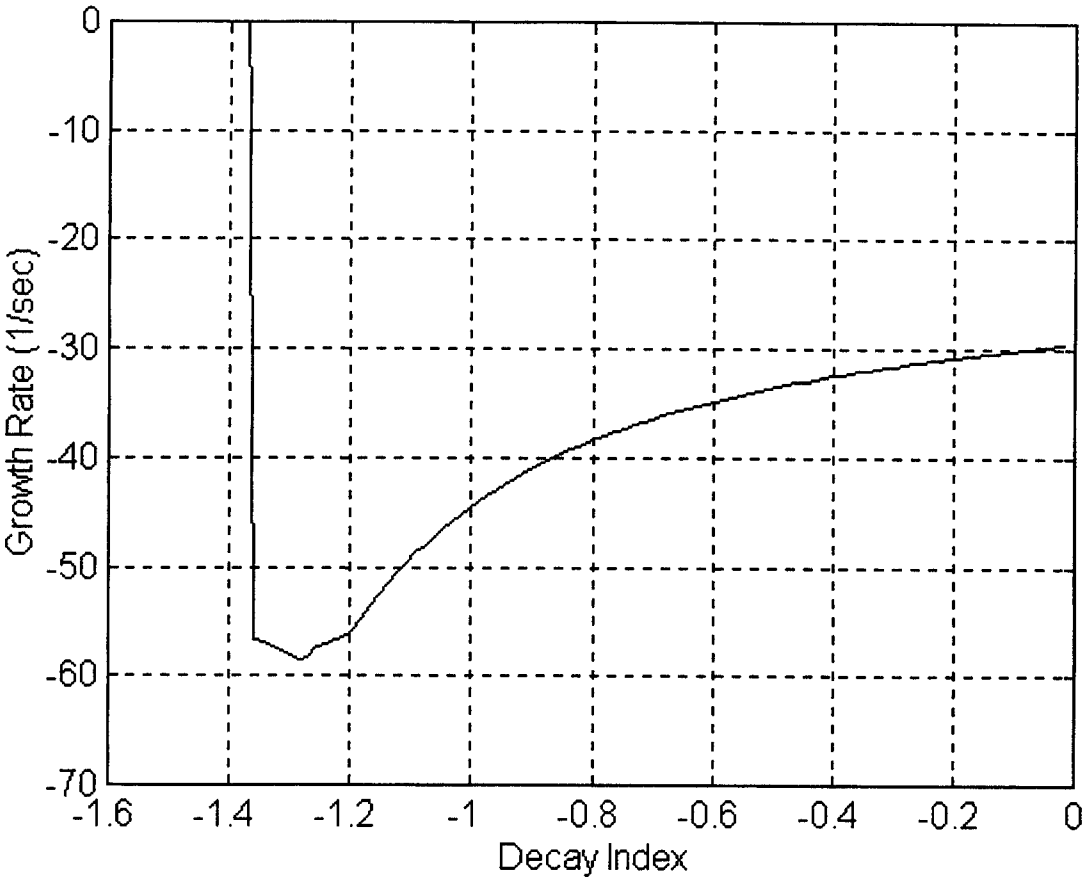

Figure 5.6 Robustness graph for EFC PD system. The PD systems never go above -10 (1/sec) as the decay index approaches 0. Both of the PD systems were designed to operate at a decay index of n_i=-1.32.

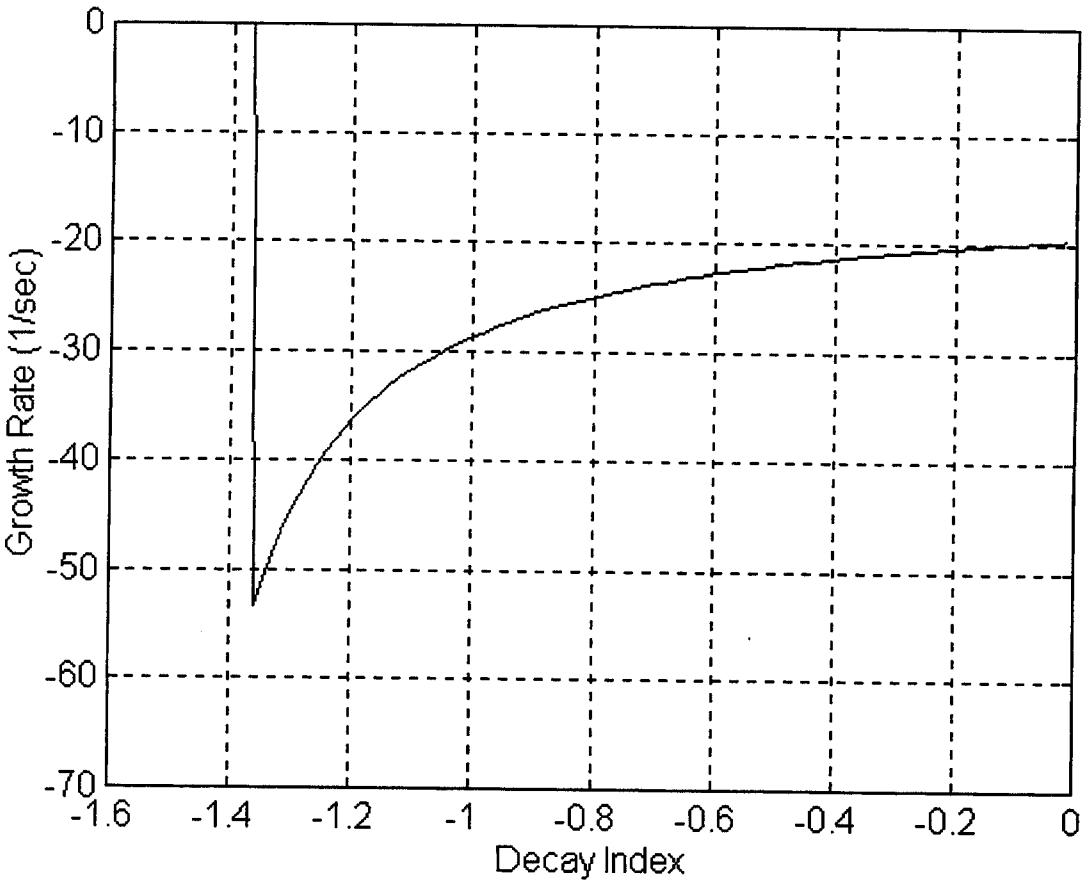

Figure 5.7 Robustness graph for OH2 PD system.

System Analyzed	Max. Growth Rate Controlled	Min. n_i where γ>-10 (1/sec)	Max n_i at limits of stability
EFC FSFB	1560 (1/sec)	-0.40	-1.357
OH2 FSFB	2570 (1/sec)	-0.81	-1.397
EFC PD	1860 (1/sec)	NA	-1.372
OH2 PD	1770 (1/sec)	NA	-1.367

Table 5.1 Range of Control for FSFB gain selection system.

5.2 EIGENMODE ANALYSIS

Robustness limits were established by tracing the real value of the vertical growth mode against a change of decay index, n_i. The power supply time constant was set at 3000 1/sec to approximate the delay time of the chopper power supply. The gain matrix, **K,** and gain values P and D were held constant during the robustness calculations. The numerical results are shown in table 5.1, while figures 5.4 to 5.7 show the time constant of the slowest growth mode against the decay index for each system. The discontinuity in figures 5.4 to 5.7 is caused by a fast mode that quickly becomes positive at the maximum index. Figure 5.3 shows a graph of this mode against the slow mode that describes most time dependant behavior. Because of the two different power supply models used, the numbers in table 5.1 are not directly comparable between the FSFB control method and the PD method. It is possible to compare the general performance of each system against each other.

Overall, the PD systems worked over the widest range of operating conditions. This is most likely because the changing n_i has a large effect on the state space model, making the FSFB tracking less effective for positions away from its design point. The only aspect of the z position behavior that is affected by n_i was the rate of motion, having less effect on the PD control laws.

The fastest growth mode controlled was achieved by the OH2 FSFB system. On the other hand, this result is different from the PD systems comparison, where there was little difference in the maximum growth rate controlled by each coil set. The discrepancy is explained by how each system is developed. The FSFB gain calculation is highly dependent upon the state space model used. Since the input matrix, **B**, is substantially different for each coil set, the performance results can vary widely. The PD system only works on the z position output, which remains the same for each coil set. Both EFC control systems had the least degradation in performance for a changing n_i, which translates into the most resistance to changes in the plasma.

5.3 TIME DOMAIN ANALYSIS

For each system there were several values of n_i where the time performance was examined. Figures 5.8 to 5.18 show several selected results. The idea behind time domain analysis is to realize the exact performance of the system. Eigenmode analysis gives us approximations of time domain performance. The settling time is related to the eigenmode analysis as $T_s \leq 4\gamma$, with γ representing the real time constant of the slowest growth eigenmode. Faster growth modes may speed up the settling time, so this is only an upper bound on performance. The rise time, T_r, is a function of the absolute value of certain growth modes. The percent overshoot, O_S, is related to the ratio of the imaginary value over the real value of certain growth modes. Formulas for the last two values exist for two pole models, but the 50 poles present in our state space model preclude accurate prediction of time performance by the

Control System	Overshoot (%)	Rise time	Settling time
EFC FSFB	0%	56 ms	130 ms

Control System	Overshoot (%)	Rise time	Settling time
OH2 FSFB	1%	38 ms	60 ms
EFC PD	95%	0.6 ms	80 ms
OH2 PD	180%	0.8 ms	100 ms

Table 5.2 This lists the time domain performance results for each system taken at n_i=-1.32, which has an uncontrolled growth rate of 1065 (1/sec).

eigenmodes. The results from the graphs show that the state space systems have the best damping, which is marked by the absence of overshoot and much slower rise times. These systems hold the plasma in position with minimal oscillations. The PD systems do not do so well in this regard, with large overshoot and two orders of magnitude difference between the rise time and settling time. These numbers are suspect because the rise time is only slightly slower than the modeled power supply time of 0.333 ms. Figure 5.19 shows that the voltage produced by the D term is much quicker than the power supply and gives the PD system an artificial rise time. What these numbers and the graphs show is that the FSFB systems are able to damp the faster growth modes, while the PD system falls short in that respect. Since these modes decay quickly, they do not hurt the stability of the system, but they will contribute to overshoot, even with a more accurate power supply model.

The settling times of the systems, with the exception of the OH2 FSFB, were within 10 ms of the prediction based upon the slowest growth mode. The OH2 FSFB had a predicted T_s=170 ms, which is very different from the time on Table 5.2. A faster mode that affects the z position dominates over the slower mode in this case. This brought up the question if the slowest growth mode was an accurate predictor for the minimum operating range. Figures 5.8 and 5.11 show the FSFB systems operating at the minimum n_i range shown in table 5.1. Both graphs

show systems dominated by the slowest growth mode at that point, proving the utility of the robustness graphs.

What the time domain analysis shows is that for a plasma with low n_i a single slow growth mode dominates. As n_i becomes more negative, complex higher order modes grow in magnitude and add oscillations to the system. The FSFB system gain selection method is able to keep these modes damped over a larger range of plasma conditions, while in the PD systems they surface readily. As each system approaches its stability limit, one higher order mode gains a positive real root. Figure 5.9 shows the growth mode driving the z position to instability at a slow rate. The system at this point is exceptionally sensitive to changes in n_i and quickly approaches the uncontrolled growth rate.

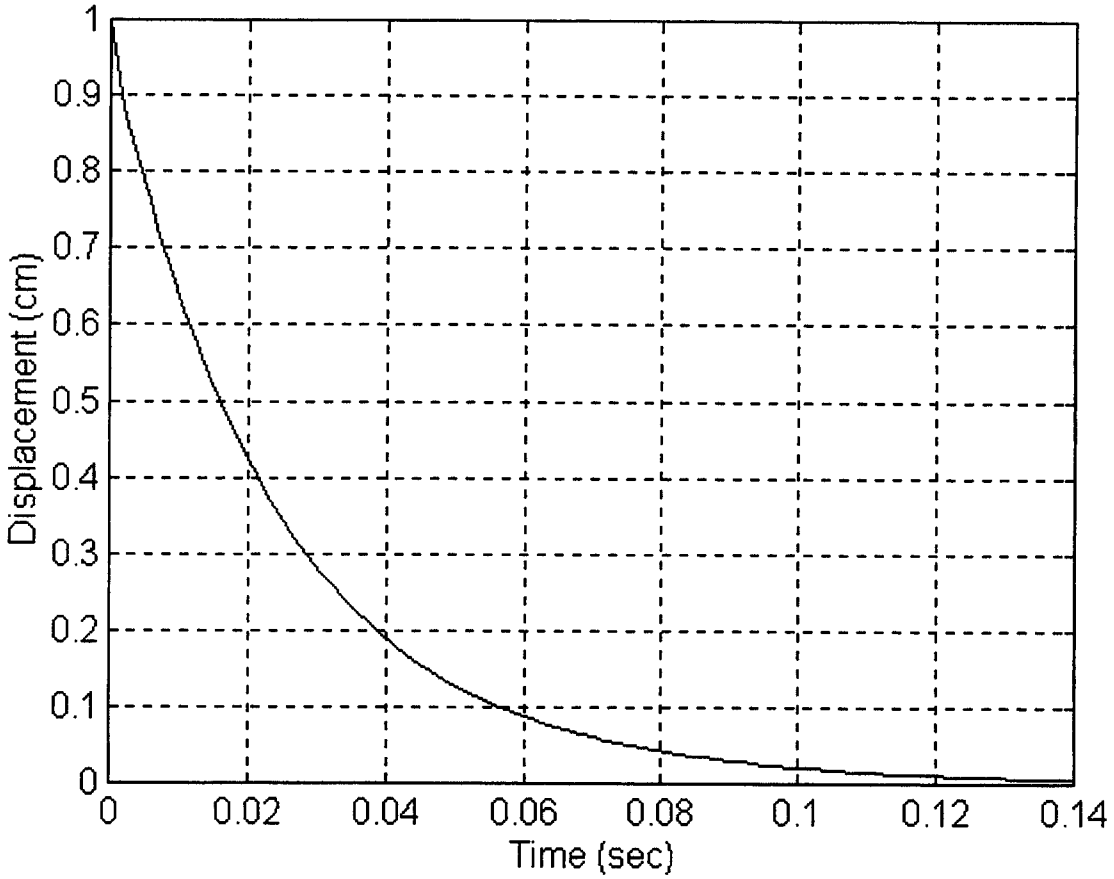

Figure 5.8 EFC FSFB system time performance at n_i=-1.32.

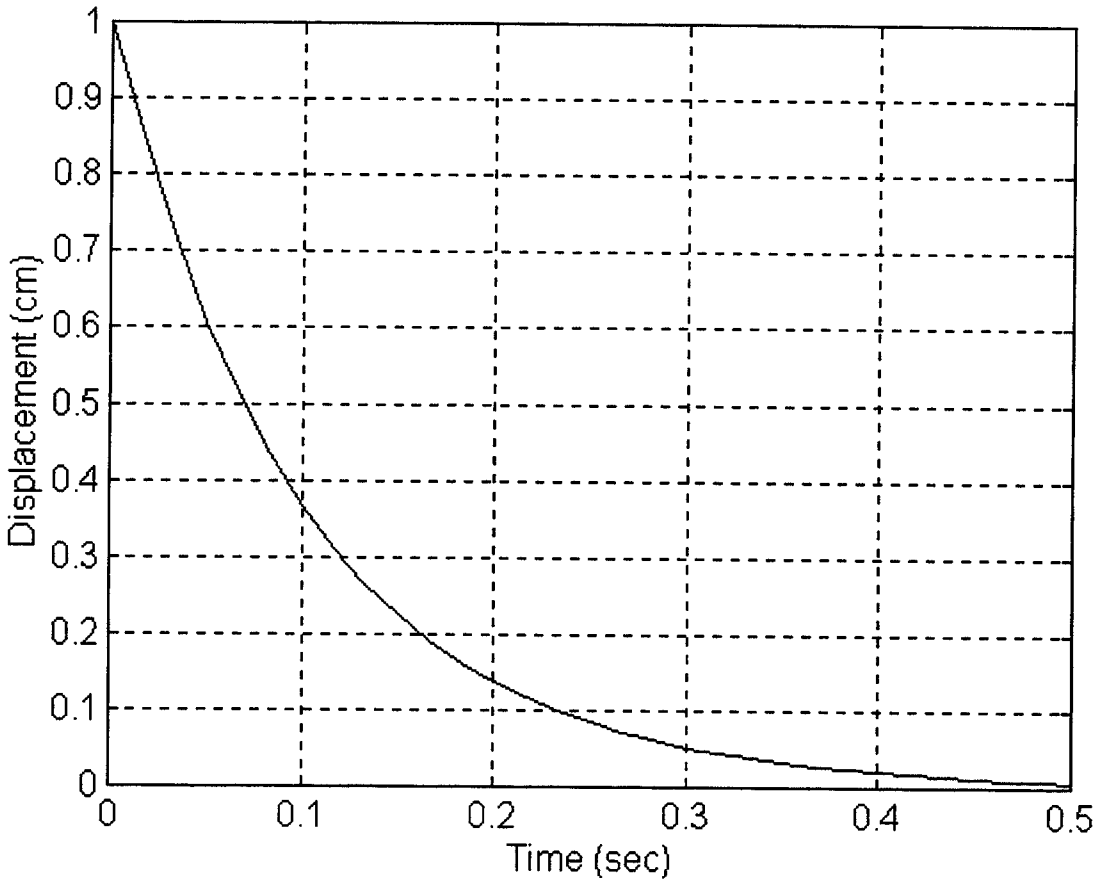

Figure 5.9 EFC FSFB system time performance at n_i =-0.40. This is the lower limit of system performance for the EFC system, with γ=-10 (1/sec) and T_s=0.4 sec.

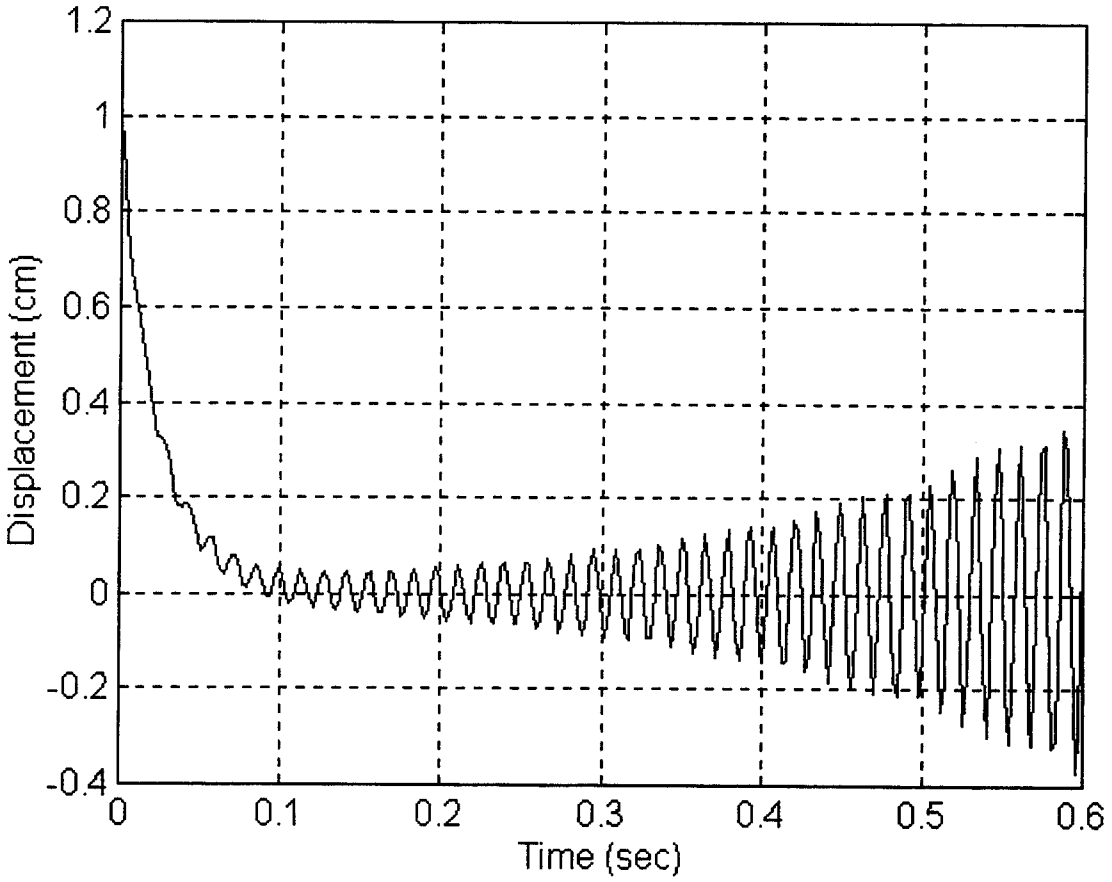

Figure 5.10 EFC FSFB system time performance for n_i=-1.357. This system has gone unstable. All systems failed in the same way, with a oscillating mode that grows to infinity.

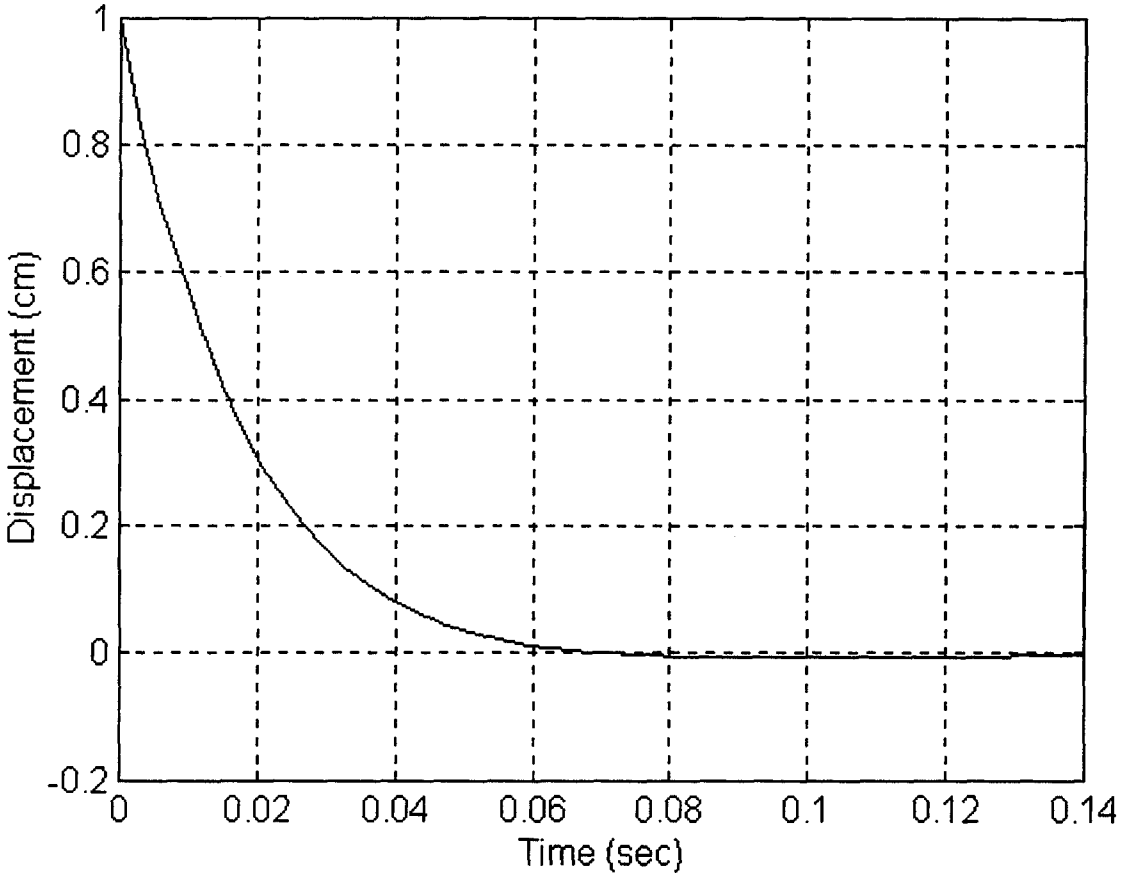

Figure 5.11 OH2 FSFB system time performance for n*=-1.32. The slowest growth mode is 28 (1/sec), which is much slower than the time performance of this system, listed in table 5.2. A faster growth mode is dominating the result.

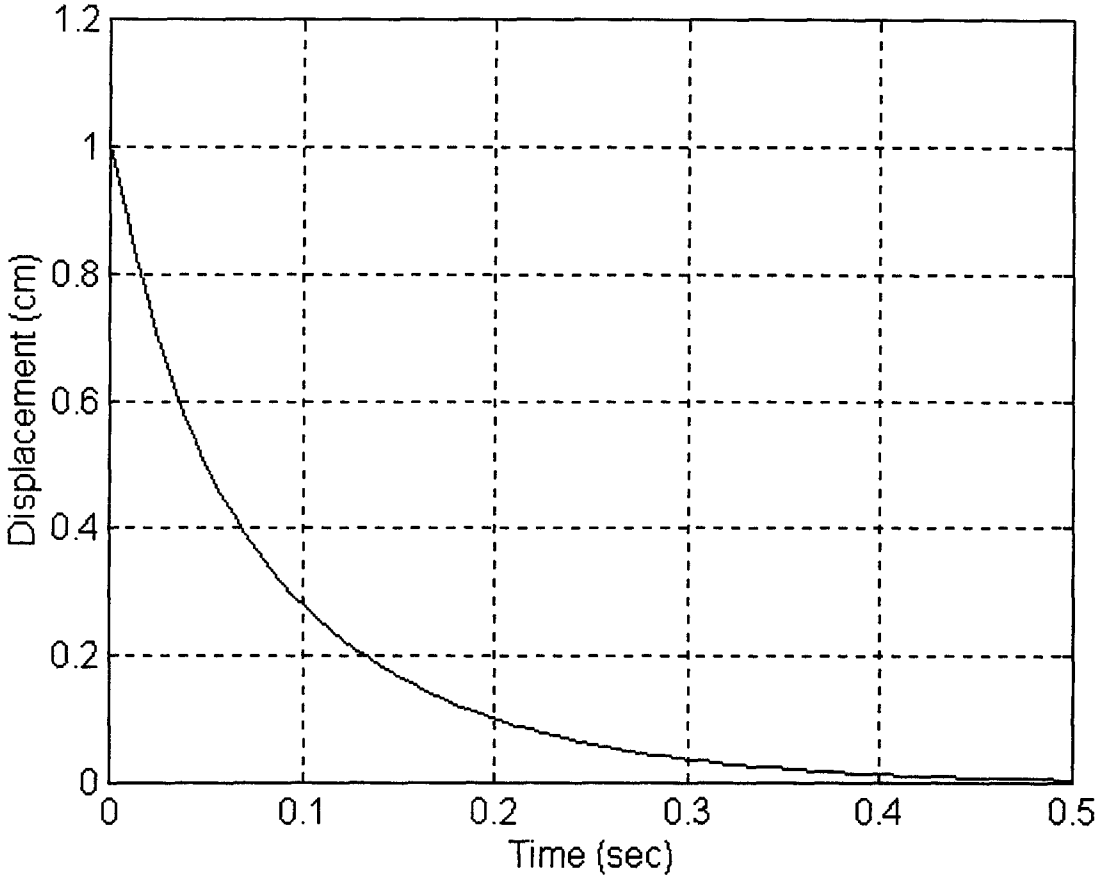

Figure 5.12 OH2 FSFB system time behavior for n_i=-0.81. T_s=0.4 sec, which is the predicted time for the lowest growth mode at this point of 10 (1/sec).

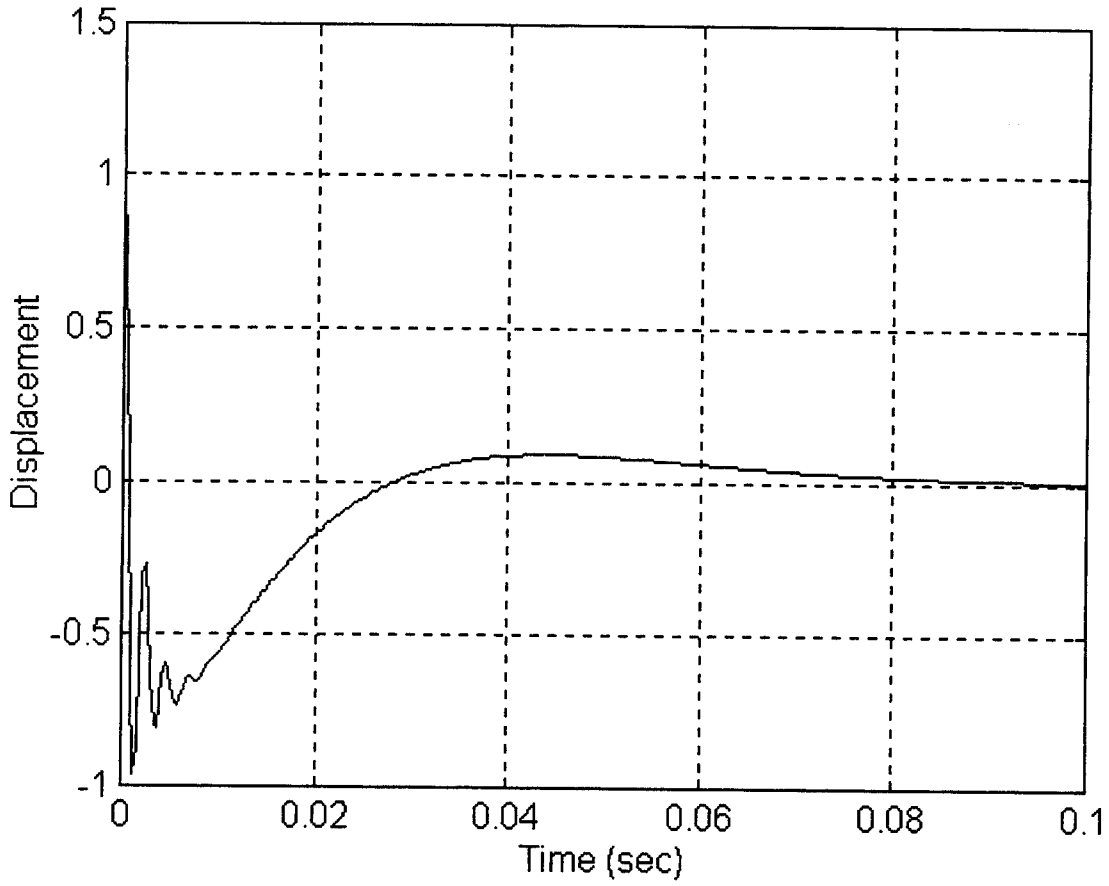

Figure 5.13 EFC PD system time performance for n_i=-1.32. The large overshoot comes from a high order mode in the system. After 10 ms, that mode decays and the designed PD overshoot performance occurs at t=0.04 sec.

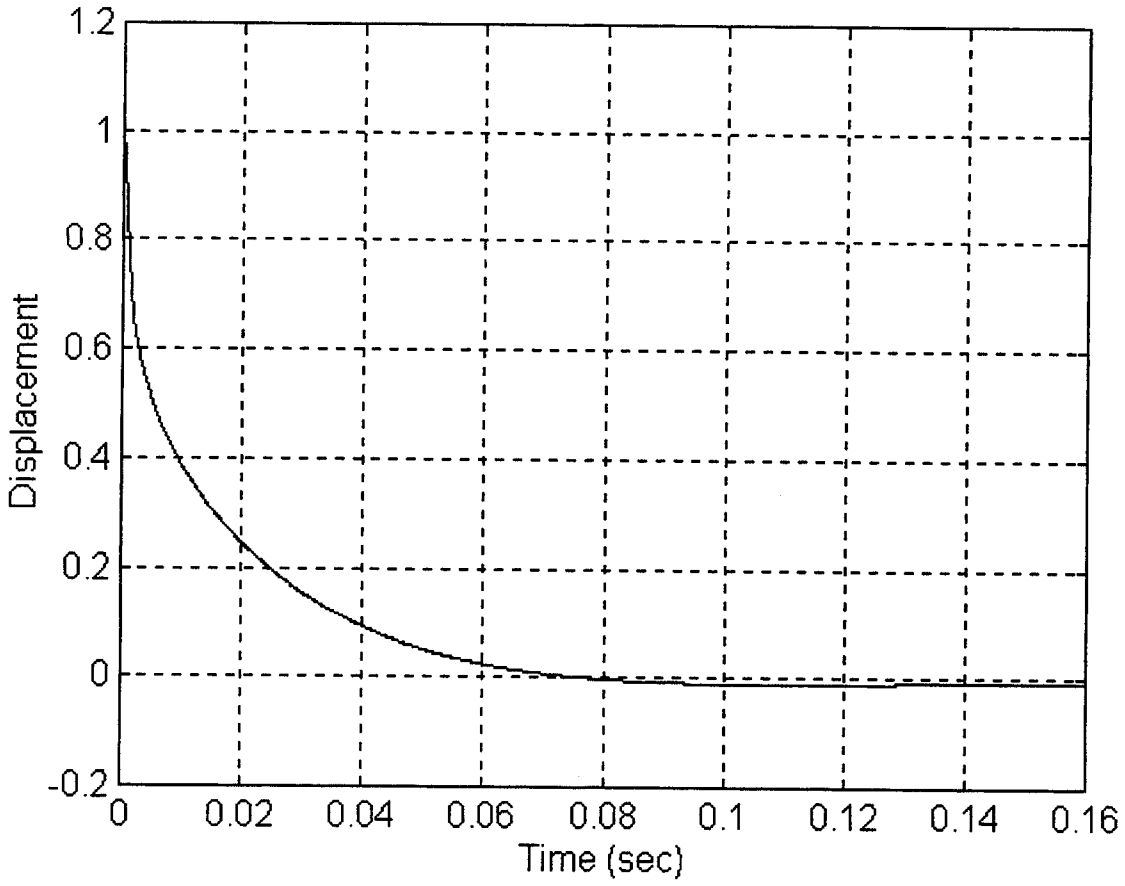

Figure 5.14 EFC PD system time performance for n_i=-0.01. This graph shows how the lower order modes disappear as n_i approaches 0.

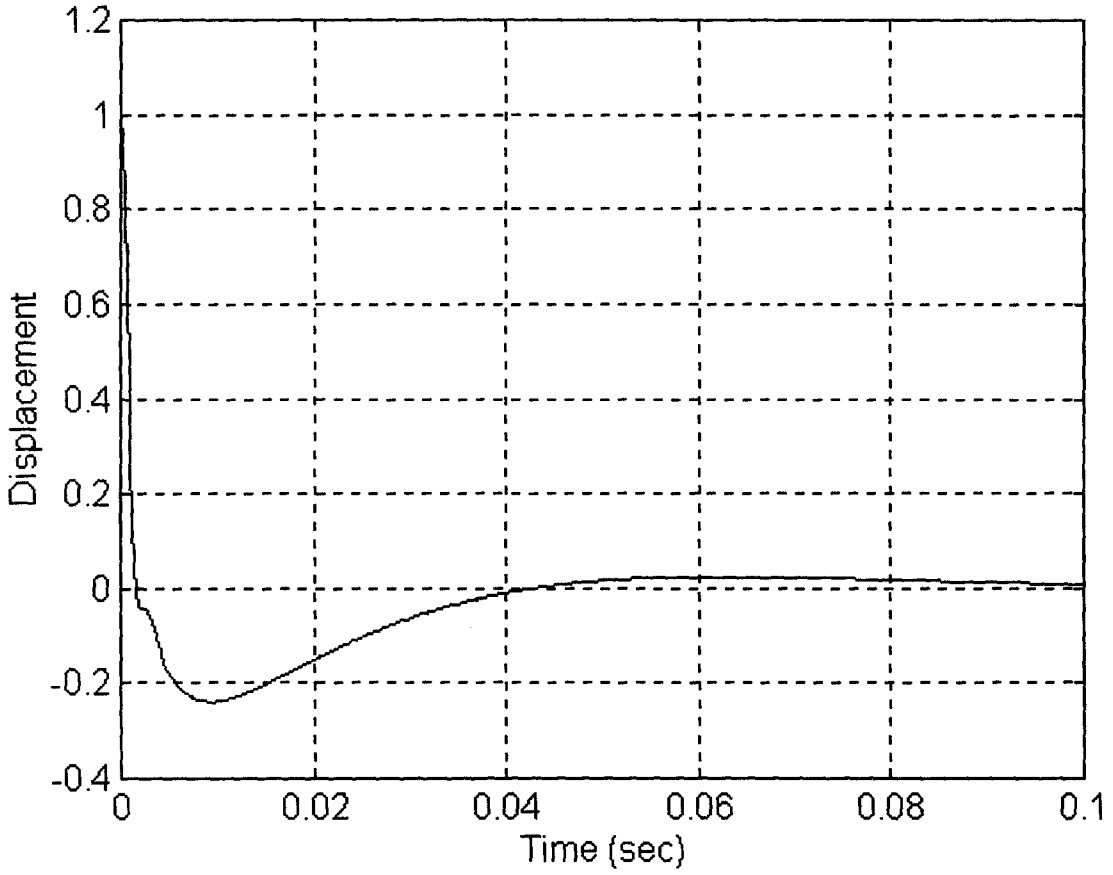

Figure 5.15 EFC PD system time performance for n_i=-1.08, which has an uncontrolled growth rate of 200 (1/sec). At this range the PD control systems have reasonable performance.

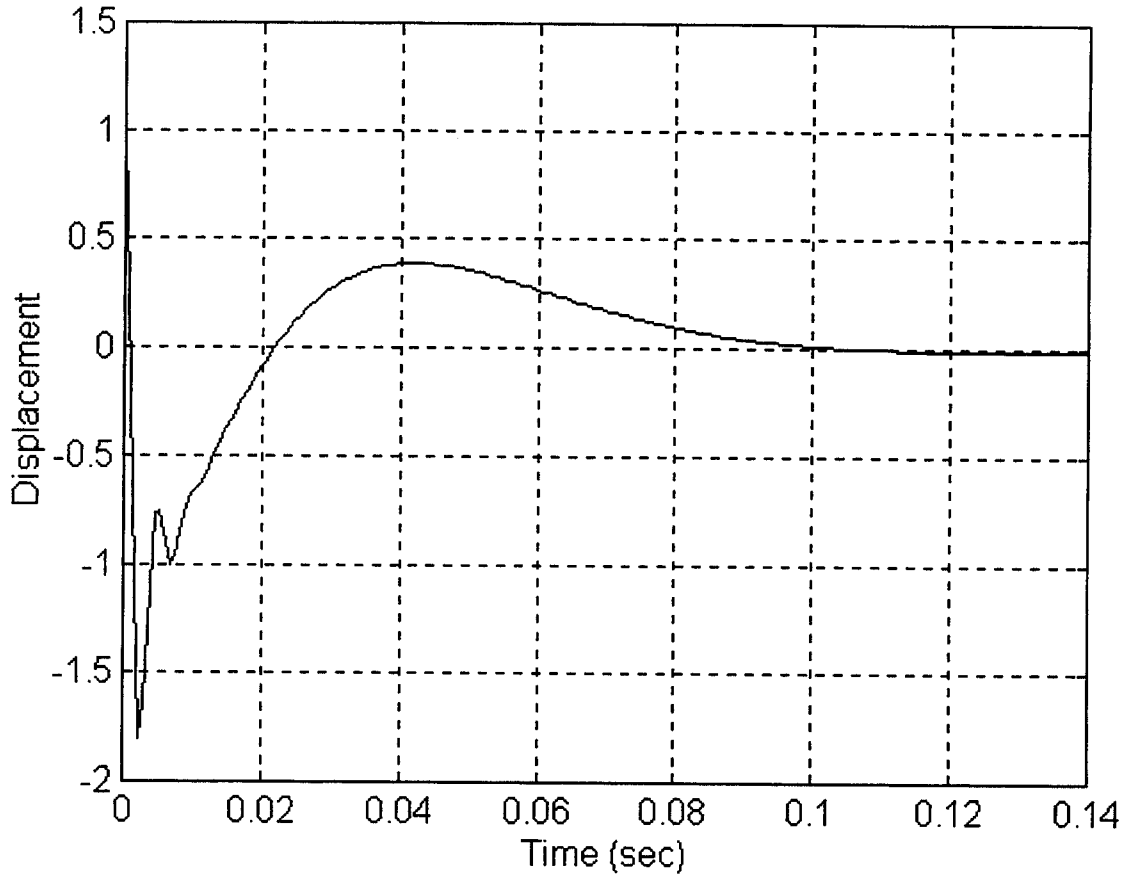

Figure 5.16 OH2 PD system time performance for n_i=-1.32.

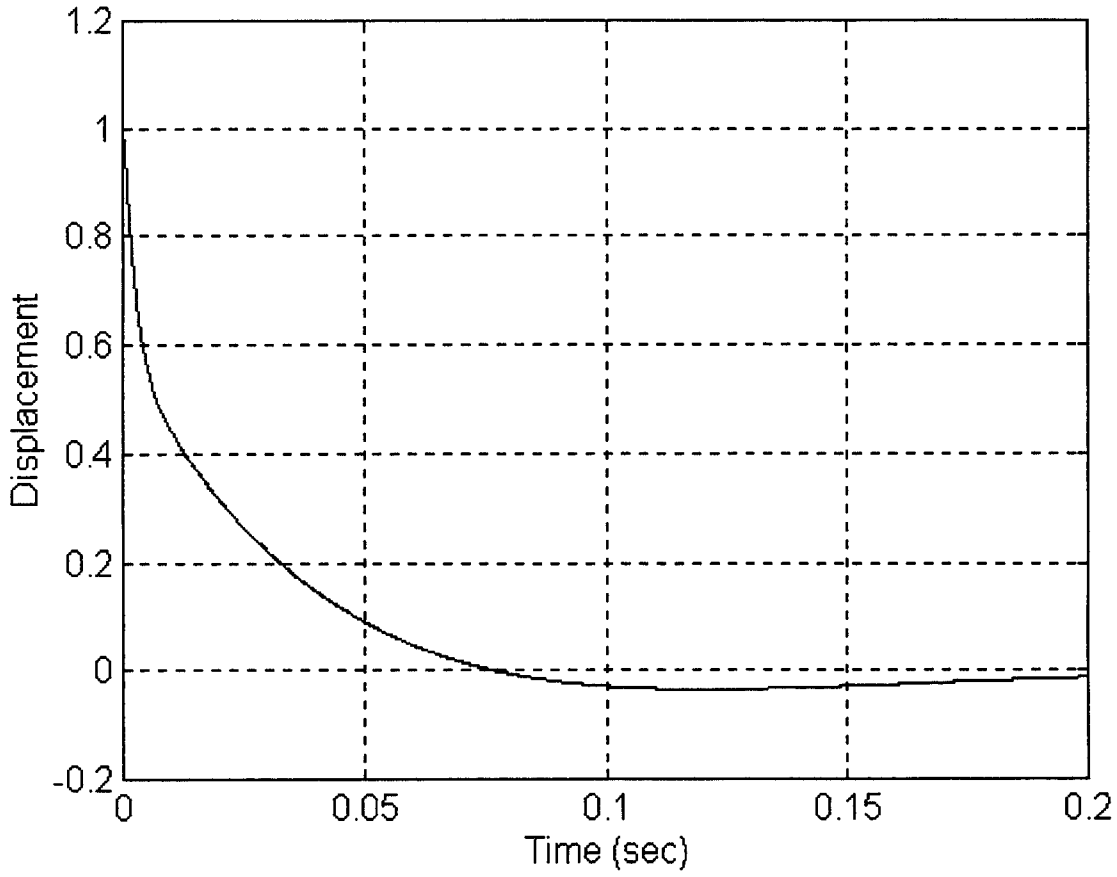

5.17 OH2 PD system time performance for n_i=-0.01.

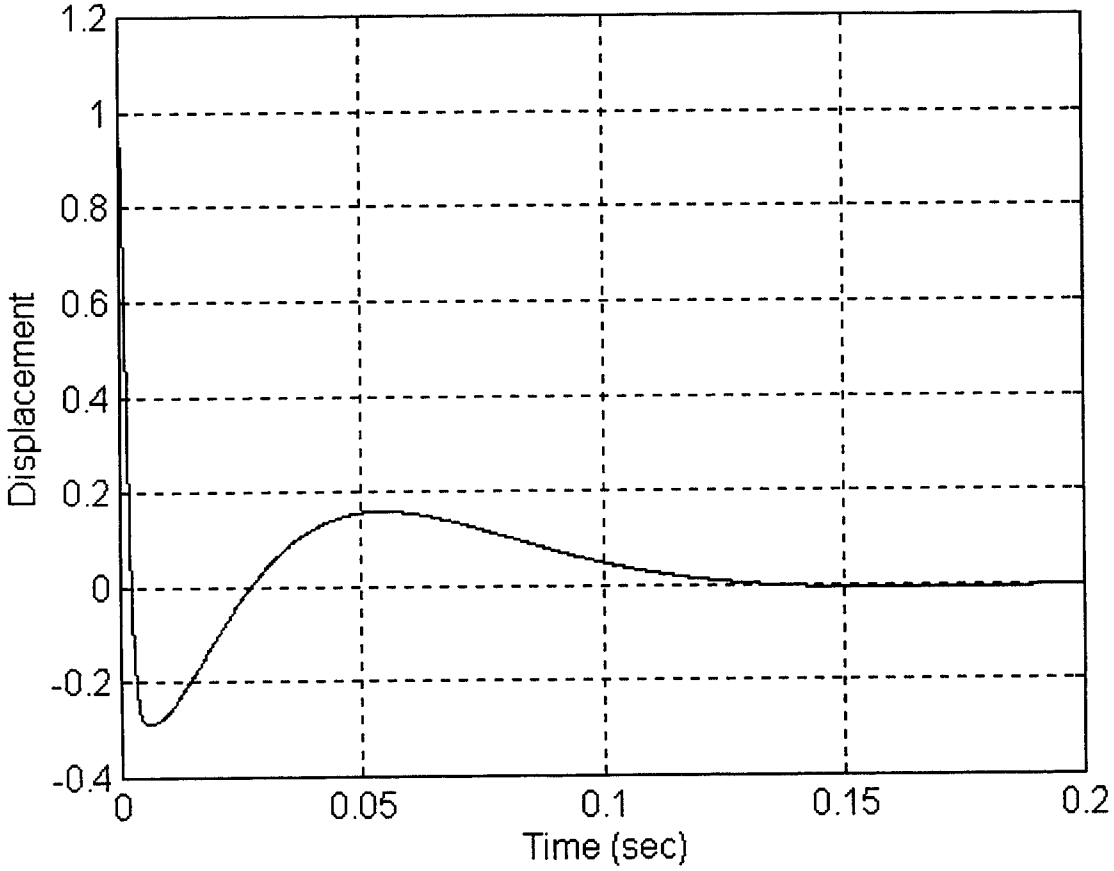

5.18 OH2 PD system time performance for n_i=-1.08.

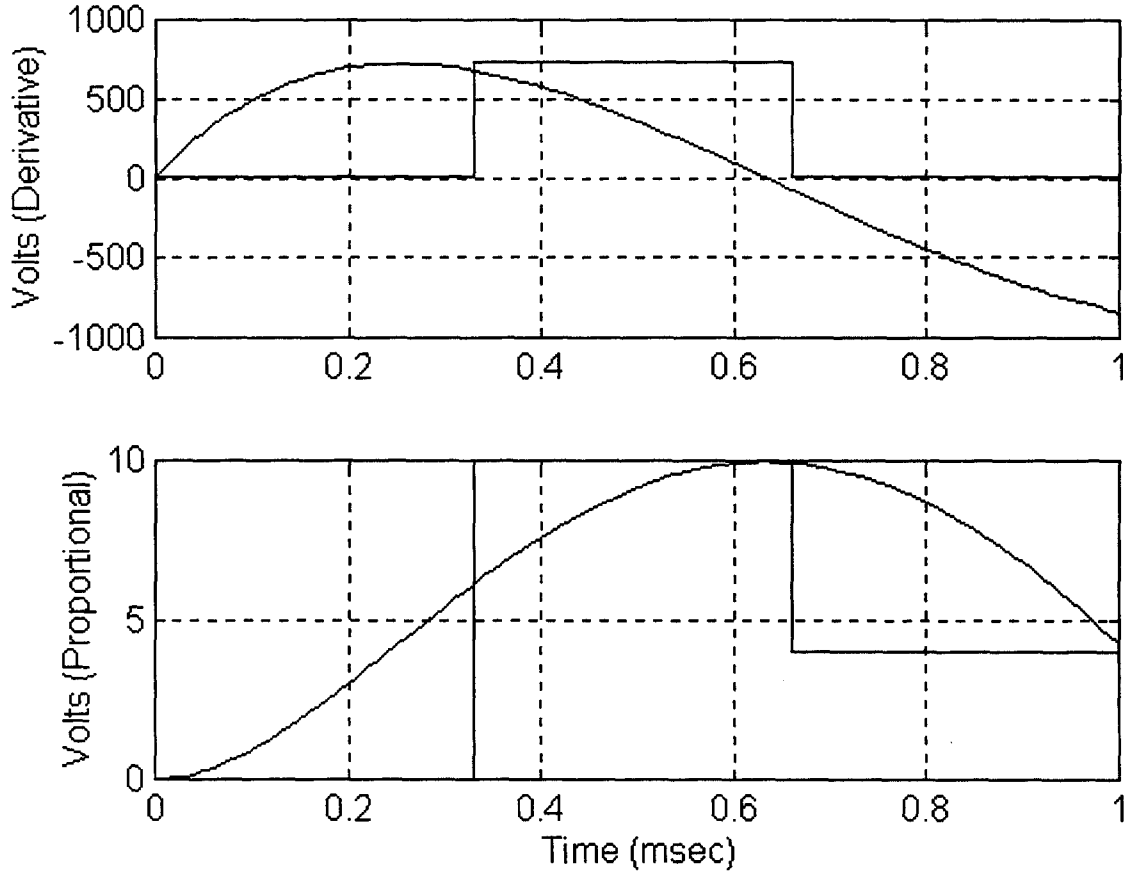

Figure 5.19 Graph of the P and D actual and predicted voltage signal for EFC control at n_i=-1.32, which corresponds to the time performance in figure 5.13. The speed of the derivative drives the PD response faster than the power supply moves, giving a false account of rise time and overshoot.

CHAPTER 6

CONCLUSIONS

This work has investigated alternate methods of controlling the vertical position of the plasma in the ALCATOR C-Mod Tokamak. The full state feedback (FSFB) method represents a different type of control system from the proportional-derivative (PD) approach. Add to that the option of initiating control through the OH2 coil and there are three new methods investigated with one old method compared(EFC PD). A point design for a power supply connecting transformer was developed that takes into account the electrical, magnetic, thermal, and stress conditions. The rigid filament model provided a linear system for the development and comparison of control systems. A linear power supply was created to use in the model. Once the control gains were selected and applied to the linear system, the eigenmode solution and time performance provided enough information to recommend control options.

6.1COUPLING TRANSFORMER DESIGN

The transformer design capable of adding an additional fast power supply to the OH2 circuit was created through existing engineering principles. It turned out to be 1 m tall with 0.42 m radius, providing a manageable size to for incorporation in the ALCATOR C-Mod power supplies. There is no doubt that this device can be built, but the benefits of using the transformer have yet to be established. Literature research did not find examples of a transformer being used to couple power supplies for fast control, so the concept requires further investigation before it is proved. If the principles work well, it will provide an alternate design for fast power supplies with high amperage.

6.2 PROPORTIONAL-DERIVATIVE CONTROL

Using PD control there is no clear advantage to using the OH2 coils. The EFC coils have a slight advantage in speed of phenomena controlled when compared to PD control through the OH2 coils. PD control systems also had the most robustness with respect to changes in the decay index, when compared with the FSFB control. Also, the PD systems were more robust with respect to a change in the power supply model. This, along with the reduced needs of an observer, means that the PD system is the easiest to implement on the ALCATOR C-Mod tokamak.

The one problem that the PD system displayed was an inability to damp higher order modes. This is caused by trying to control a system with fifty modes by using only two gains. It is noted that the PD power supply model did induce an artificially fast response time and large overshoot, suggesting that time domain performance is better than the model in this thesis

provides. Overall, the PD EFC control should be continued if the proposed experiments run on the machine will not have problems with damping.

6.3 FULL STATE FEEDBACK

The best method for implementing FSFB control is through the OH2 coils. The large amount of gains in the **K** matrix allow more control over most of the modes, and it is believed that the OH2 coils provide better access to stabilizing currents in the vacuum vessel. The other advantage to FSFB is the ability to damp higher order modes in the time performance of the system. This limits overshoot and slows down the response of the control system

FSFB does have problems with robustness. State space control is much more dependent upon a linear model than PD systems, and changes in that model have a much stronger effect on the control system. The FSFB system also failed to control when the PD power supply model was used. This would require FSFB systems to be developed taking into account the characteristics of the power supply in order to prevent instabilities. Estimation of the states provides another disadvantage to FSFB control, for it will most likely require a new control computer to take full advantage of controlling a large number of modes. The FSFB OH2 control should be adopted only if more damping is required in machine operation.

6.4 FOLLOW ON RESEARCH

Further research only needs to be carried out if the implementation of OH2 FSFB control is desired. The most important area of examination is the effects of the coupling transformer on the control abilities of the chopper power supply. It may turn out that the coupling concept reduces the effectiveness of moving the control inboard. Furthermore, different

estimator options need to be investigated fully to determine if FSFB can predict states for our model with proper noise rejection. An alternative to improve the robustness of FSFB systems is to use gain scaling, where the **K** matrix is changed based upon the condition of the plasma. This would allow the gain matrix to stay within an adjusting linear model.

WORKS CITED

[1] Troyon, F., et al., "MHD-limits to Plasma Confinement", Plasma Physics and Controlled Fusion, **26** (1984) 209

[2] Hutchinson, Ian H., β limits, MIT 22.602 Course Notes

[3] Ward, D.J., Hofmann, F., "Active Feedback Stabilization of Axisymmetric Modes in Highly Elongated Tokamank Plasmas", Nuclear Fusion, **34** (1994) 401

[4] Humphreys, David A., Hutchinson, Ian H., "Axisymmetric magnetic Control Design in Tokamaks Using Perturbed Equilibrium Plasma Response Modeling.", Fusion Technology, **23** (1993) 167

[5] Mukhovatov, V.S., Shafranov, V.D., "Plasma Equilibrium in a Tokamak", Nuclear Fusion, **11** (1971) 605

[6] Lister, J.B., Martin, Y., Moret, J.M., "On locating the Polodial Field Coils for Tokamak Vertical Position Control.", Nuclear Fusion, **36** (1996) 1547

[7] Dorf, Richard C., Bishop, Robert H., Modern Control Systems, Addison-Wesley, (1995)

[8] Albanese, R., Coccorese, E., Rubinacci, G., "Plasma Modeling for the Control of Vertical Instabilities in Tokamaks", Nuclear Fusion **29** (1989) 1013

[9] Hutchinson, Ian 'Inertial' Cooling MIT 22.602 Course Notes

[10] Griffiths, David J. Introduction to Electrodynamics Prentice-Hall (1992)

[11] Lindeburg, Michael R. Engineer-in-training Reference Manual Professional Publications (1992)

[12] Watson, J.K. Applications of Magnetism John Wiley & Sons, (1980)

[13] Grossner, Nathan R. Transformers For Electronic Circuits McGraw-Hill (1983)

[14] Connelly, F.C. Transformers, Their Principles and Design For Light Electrical Engineers Sir Isaac Pitman & Sons (1950)

[15] Stigant, S. Austen, Franklin, A.C., The J&P Transformer Book Halsted Press (1973)

[16] Phipps, James K., Nelson, John P, Sen, Pankaj K., "Power Quality and Harmonic Distortion on Distribution Systems", IEEE Transactions on Industry Applications **30** (1994) 476

[17] Pierce, Linden W., "Transformer Design and Application Considerations for Nosinusoidal Load Currents ", IEEE Transactions on Industry Applications, **32** (1996) 633

[18] Mukhovatov, V.D, Shafranov, I.V.,"Plasma Equilibrium in a Tokamak", Nuclear Fusion, **11** (1971) 605

[19] Lazarus, E.A., Lister, J.B., Neilson, G.H.,"Control of the Vertical Instability in Tokamaks", Nuclear Fusion, **30** (1990) 111

[20] Mayr, Otto, The Origins of Feedback Control, M.I.T. Press (1970)

[21] Bennett, S., "The Development of the PID Controller", IEEE Control Systems, December (1993) 58

[22] Sontag, E.D. Mathematical Control Theory, Springer-Verlag (1990)

[23] Szidrovszky, Ferenc, Bahill, A.Terry, Linear Systems Theory, CRC Press (1998)

[24] Lublin, Leonard, Athans, Michael, "Linear Quadratic Regulator Control", In The Control Handbook, W.S. Levine ed., CRC Press (1996)

[25] Geerts, A.H.W., Hauts, M.L.J., "Linear-Quadratic Problems and the Riccati Equation", In Perspectives in Control Theory, B. Jakubczyk ed., Birkhäuser (1990)